(4)

THE BRADLEY DEPARTMENT OF ELECTRICAL ENGINEERING

VIRGINIA TECH

INTRINSIC MECHANISMS OF MULTI-LAYER CERAMIC CAPACITOR FAILURE

FINAL REPORT

Time Period: 3/15/83-5/14/88
ONR Contract No. N00014-83-K-0168
Principal Investigator: L. C. Burton

July 1988

Departments of Electrical Engineering and Materials Engineering
Virginia Polytechnic Institute and State University
Blacksburg, VA 24061

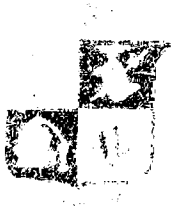

VIRGINIA POLYTECHNIC INSTITUTE AND STATE UNIVERSITY
Blacksburg, Virginia 24061 (703) 961-6646

INTRINSIC MECHANISMS OF MULTI LAYER CERAMIC CAPACITOR FAILURE

FINAL REPORT

Time Period: 3/15/83-5/14/88
ONR Contract No. N00014-83-K-0168
Principal Investigator: L. C. Burton

July 1988

Departments of Electrical Engineering and Materials Engineering
Virginia Polytechnic Institute and State University
Blacksburg, VA 24061

SECURITY CLASSIFICATION OF THIS PAGE

ADA199113

REPORT DOCUMENTATION PAGE

Form Approved
OMB No. 0704-0188

1a. REPORT SECURITY CLASSIFICATION Unclassified	1b. RESTRICTIVE MARKINGS
2a. SECURITY CLASSIFICATION AUTHORITY	3. DISTRIBUTION/AVAILABILITY OF REPORT Approved for Public Release Distribution Unlimited
2b. DECLASSIFICATION/DOWNGRADING SCHEDULE	
4. PERFORMING ORGANIZATION REPORT NUMBER(S)	5. MONITORING ORGANIZATION REPORT NUMBER(S)
6a. NAME OF PERFORMING ORGANIZATION VPI & SU 6b. OFFICE SYMBOL (If applicable)	7a. NAME OF MONITORING ORGANIZATION
6c. ADDRESS (City, State, and ZIP Code) EE Dept. Blacksburg, VA 24061	7b. ADDRESS (City, State, and ZIP Code)
8a. NAME OF FUNDING/SPONSORING ORGANIZATION Office of Naval Research 8b. OFFICE SYMBOL (If applicable)	9. PROCUREMENT INSTRUMENT IDENTIFICATION NUMBER N00014-83-K-0168
8c. ADDRESS (City, State, and ZIP Code) 800 N. Quincy St. Arlington, VA 22217	10. SOURCE OF FUNDING NUMBERS PROGRAM ELEMENT NO. / PROJECT NO. / TASK NO / WORK UNIT ACCESSION NO.

11. TITLE (Include Security Classification)
Intrinsic Mechanisms of Multilayer Ceramic Capacitor Failure

12. PERSONAL AUTHOR(S)
L. C. Burton

13a. TYPE OF REPORT	13b. TIME COVERED	14. DATE OF REPORT (Year, Month, Day)	15. PAGE COUNT
Final	FROM 3/15/83 TO 5/14/88	1988 July	

16. SUPPLEMENTARY NOTATION

17. COSATI CODES			18. SUBJECT TERMS (Continue on reverse if necessary and identify by block number)
FIELD	GROUP	SUB-GROUP	Multilayer Capacitors; Degradation & Reliability; Ferroelectric Ceramic; Leakage Currents; MLC Capacitor; Failure Modelling

19. ABSTRACT (Continue on reverse if necessary and identify by block number)

Studies related to leakage currents and intrinsic degradation of multilayer ceramic capacitors and related materials were performed.

For the X7R materials studied, the following results confirmed that the charge carrier for current is the electron: constant leakage current; negative thermoelectric voltage; negligible galvanic voltage; presence of space charge limited current. Mobilities were found to be less than $10^{-6}cm^2/Vsec$, thermally activated, and characteristic of small polaron hopping transport.

Thermal activation energies decreased with voltage for barrier layer, COG and Z5U types, but not for X7R. Such voltage dependence, accompanied by superohmic current, is indicative of grain boundary (GB) dominated transport. Complex impedance plots give evidence of several resistive contributions, which could be attributed to grains and GB. Modelling of GB impedance indicates the importance of grain size homogeneity and grain curvature. However, the role of GB related to the resistance and degradation of these materials was not

20. DISTRIBUTION/AVAILABILITY OF ABSTRACT	21. ABSTRACT SECURITY CLASSIFICATION	
☒ UNCLASSIFIED/UNLIMITED ☐ SAME AS RPT. ☐ DTIC USERS		
22a. NAME OF RESPONSIBLE INDIVIDUAL	22b. TELEPHONE (Include Area Code)	22c. OFFICE SYMBOL

DD Form 1473, JUN 86 *Previous editions are obsolete.* SECURITY CLASSIFICATION OF THIS PAGE

19. ABSTRACT (continued)

conclusively established.

Degradation studies were made on Z5U and X7R devices. Currents most commonly increase exponentially with time, as $\exp(\beta t)$, where the rate constant β increases exponentially with temperatures for both types; β increases with voltage as a power law for Z5U, and exponentially for X7R.

The exponential time increase of current is accompanied by a linearly decreasing thermal activation energy, which can be attributed to a decrease in the hopping or GB potential. Ceramic conductivity varies exponentially with activation energy during different stages of degradation. The current-voltage power law exponent increases during degradation, and is attributed to a "smoothing" of electrode asperities resulting from ionic movement. Such movement is also evident during degradation from color gradients seen in cross sectioned pieces, and in a polarity-reversal "healing" effect that was found for Z5U, X7R and thick film devices.

Theoretical expressions for the rate constant β were derived, based on oxygen ion (and vacancy) diffusion, resulting in increased carrier concentration, and reduced transport potential barrier. The rate constant has the form

$$\beta = \frac{AV^n}{W^2} \exp\left(\frac{-E_a}{kT}\right)$$

where V = voltage, n = constant greater than unity, W = thickness, A = constant and E_a = oxygen ion mobility activation energy. The V and T dependences of this expression agree with our experimental results for Z5U devices; the V dependence is not followed by X7R. This expression agrees with the empirical results reported by Minford, and by Procopowicz and Vaskas.

TABLE OF CONTENTS

SUMMARY OF RESULTS

The studies reported here are divided into two sections: Leakage Current, and Intrinsic Degradation. The former includes transient behavior, current-voltage-temperature behavior, studies of charge carriers, and their transport. The latter includes time dependence of degradation, other degradation characteristics, and degradation models. These items are summarized below in that sequence.

1. Leakage Current: Transient Behavior

Below about 130°C, especially at low voltages (<10V), polarization currents dominate. Under DC bias, capacitance values (dielectric constant) for commercial Z5U, X7R and COG devices (and all other ceramic types measured) decrease as the logarithm of time. This results in polarization current with a time dependence of t^{-m} , where m is nearly unity near room temperature, decreasing to near zero at ~120°C, and not a strong function of voltage. This current dominates over short times, below 120°C, and is generally not correlated with conduction (transport) current. Due to hysteresis effects, the transport current for these materials cannot be reliably determined as the difference betwen polarization (charging) and depolarization (discharge) currents. The displacement current consists of extra terms due to time and voltage dependences of the dielectric constant.

2. Leakage Current: I-V-T Behavior

For all samples measured, ohmic behavior at low fields ($\simeq 10^3$V/cm) is followed by superohmic, the most common type being a power-law (V^n) with $1<n<3$. One possibility for the $V^{3/2}$ relation commonly seen is electron emission from electrode asperities, which were identified in cross sections, and are responsible for such currents in other solids. The near-square law behavior

often measured for degraded devices is attributed to a "dulling" of these electron emission points by localized ion movement.

Activation energies decrease with voltage for all types measured other than X7R, accompanied by super-ohmic voltage dependence. This is indicative of GB-controlled transport, or of a voltage-dependent hopping potential barrier.

3. Leakage Current: Type of Carrier

It was confirmed that the charge carrier for current, for the type of X7R devices and blanks measured, is the electron. This assertion is based on the following: a) Leakage currents under accelerated conditions are constant with time over extended periods (several months) prior to degradation; b) Thermoelectric voltages are negative and stable; c) No Galvanic voltages could be detected for X7R blanks; theoretically predicted Galvanic voltages were measured for Y_2O_3:ZrO_2 pieces in the same apparatus; d) Space charge limited currents are attributed to electrons injected from the cathode.

4. Leakage Current: Carrier Transport

Hall voltages could not be measured for X7R pieces, even at elevated temperatures ($\simeq$200°C), due to low carrier mobility. Thermoelectric measurements confirmed the low mobility ($<10^{-6}cm^2/Vsec$) , and that thermal activation energy is dominated by mobility for both new and reduced pieces. Carrier concentrations are essentially temperature independent. These facts are consistent with small polaron hopping transport.

The role of grain boundary impedance was sought using complex impedance measurements. Evidence of grain and GB contributions were seen. Grain boundary modelling indicates the importance of grain curvature, and size homogeneity, in maintaining high ceramic impedance, if GB controlled. However, reasons are given why a strong case cannot yet be made for GB control of transport for our X7R pieces.

5. Intrinsic Degradation: Time Dependence

Most degradation measurements were made on commercial Z5U and X7R devices. The most common form of current increase with time for both types, prior to failure, is exponential ($I \sim e^{\beta t}$). Power law behavior was also seen for X7R at shorter times. For Z5U, degradation rate constant β increases as a power law with voltage and exponentially with temperature. For X7R, voltage and temperature dependence are both best fit by exponentials.

6. Intrinsic Degradation: Other Characteristics

The exponentially increasing current (with time) is accompanied by a linearly decreasing activation energy. Thermal activation energies decrease (from ~1.3eV) with degradation, being zero for severe degradation. This is attributed almost totally to transport (reduced hopping or grain boundary potential.) Ceramic conductivity varies exponentially with activation energy, except for severely degraded cases. The current-voltage power law exponent increases with degradation; we attribute this to the "smoothing" of the cathode ("virtual cathode" effect.)

For simulated degradation (reduction in hydrogen), carrier concentration and mobility both increase by orders of magnitude.

Concurrently with degradation, color gradients developed across Z5U layers. A polarity reversal "healing" effect was measured for Z5U, X7R and thick film capacitors during degradation. These effects are indicative of ionic movement.

7. Intrinsic Degradation: Models

Two models were derived for the degradation rate constant, β. These are both based on oxygen diffusion as the cause of degradation, the effects being increased carrier concentration and reduced transport potential energy barrier.

The rate constant is found to have the following voltage (V), temperature (T), and thickness (W) dependences:

$$\beta = \frac{AV^n}{W^2} e^{-E_a/kT}$$

where n is greater than unity, A=constant, and E_a is the oxygen ion mobility activation energy. If lifetime is defined as β^{-1} , the same equation obtained empirically by Procopowicz and Vaskas, and by Minford, is obtained.

1. INTRODUCTION

This report discusses work performed on ONR contract N0014-83-K-0168, "Intrinsic Mechanisms of Multilayer Ceramic Capacitor Failure" over the period of the contract, 3/15/83 to 5/14/88. The overall objectives of the program were to study fundamental (intrinsic) leakage current and degradation behavior in MLC capacitors and related material, and to model such behavior.

A variety of measurements were made to address these objectives. Since degradation and failure in an MLC device almost always means increased leakage current leading to shunt or short-circuit conditions, these measurements were aimed at understanding the nature of leakage current, and the causes for its increase with time under voltage-temperature stress. Therefore, the technical material in this report is divided up into two main sections: Leakage Current (Section 2), and Intrinsic Degradation (Section 3.)

The presentation below does not go in any particular chronological order, i.e. the order in which the work was performed. An attempt is made to present results in a manner to give the clearest picture of our findings related to MLC current and degradation.

Also, since most of this material has been presented elsewhere in greater detail (reports, publications, etc.), it is presented here in a more-or-less summary form. Please refer to the more detailed references, where noted.

2. LEAKAGE CURRENT

Leakage current is defined in this report as current caused by transport of true charge across the dielectric. This is contrasted to displacement current which is enhanced by polarization phenomena, for the DC case. For low fields the total current density J can be expressed as

$$J = \sigma E + \varepsilon_o \partial E/\partial t + \partial P/\partial t \quad (1)$$

where σ, E and P are conductivity, electric field and polarization. The first term represents leakage current and the others displacement current.

Direct voltages were used for most of our measurements, including accelerated stress on MLC devices. AC voltages were used mainly for the impedance measurements, to be discussed in Section 3. DC voltages were used for all of the measurements discussed in Section 2.

2.1 Transient Behavior

For DC studies of degradation processes, we are interested mainly in leakage (transport) current. For a high resistance dielectric near room temperature, this is difficult to measure over short to moderate time periods since it is masked by polarization current. Such transient behavior was of interest to us for several reasons: i) We had to be sure that polarization currents had decayed to zero in order to determine transport current; ii) It could be of significance with regard to low frequency impedance measurements; iii) Such transients for different materials may be of interest unto themselves.

Since polarization current results from dipole reorientation which changes polarization P, this will also be evident in capacitance, as shown in Figure 1, for a commercial $BaTiO_3$-based X7R. On semi-log plots, capacitance often varies linearly with the logarithm of time, i.e.

$$C = C_0 - C_1 \ln t \quad (2)$$

where C_o and C_1 are constants.

Polarization current I_p under DC bias can be expressed as

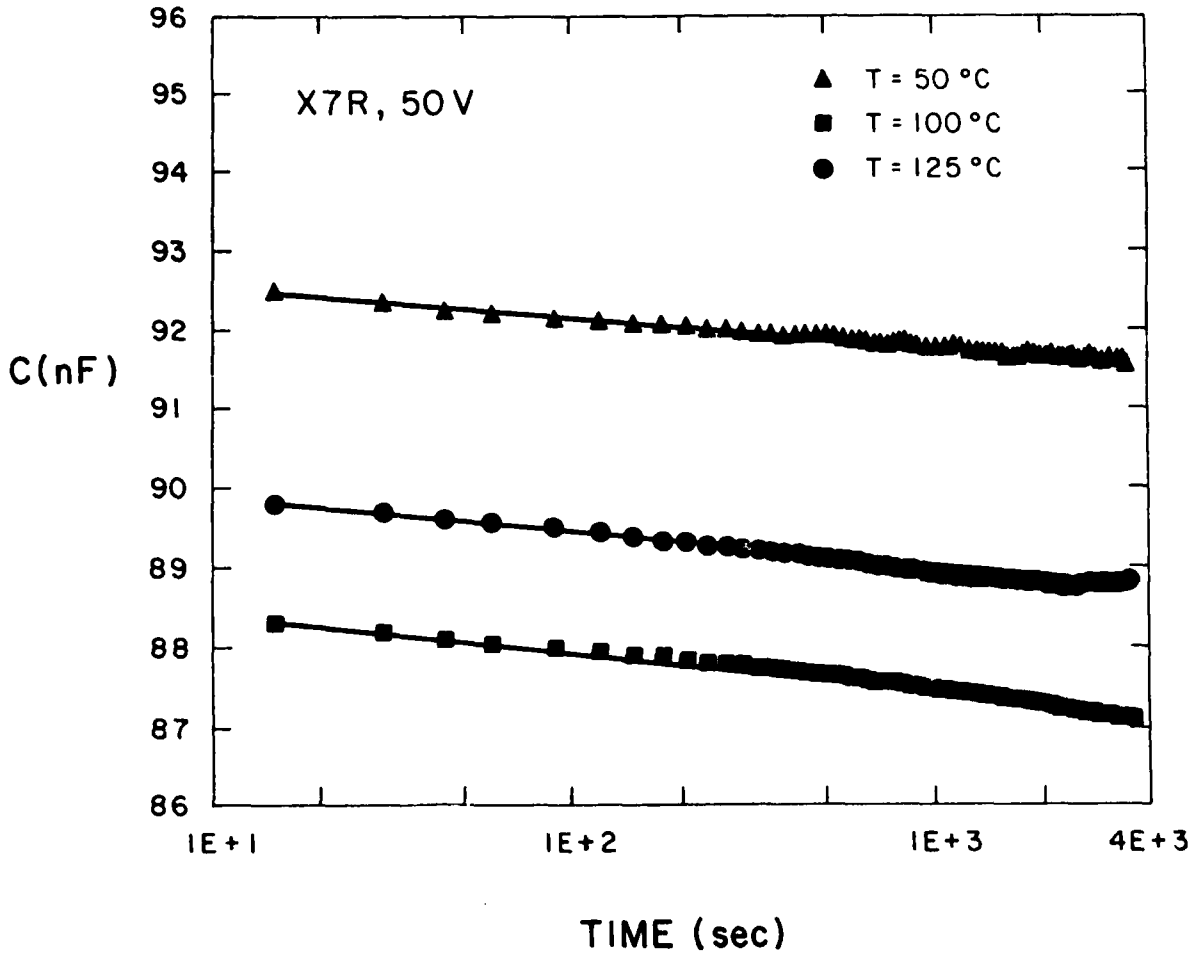

Figure 1. Decrease in capacitance with time for X7R device at three temperatures; 50V bias. The solid lines are least-square fits to the equation $C = C_0 - C_1 \ln t$.

$$I_p = dQ/dt = VdC/dt = VC_1/t \quad (3)$$

This relation is fairly closely followed at low temperatures, as seen in Figure 2. Over the time scales of these figures (about 1 hour) transport current is not evident.

Figure 3 illustrates the onset of transport current, after approximately one hour, even at elevated temperature (100°C, 20V, X7R). In principle, transport current is the difference between the magnitudes of polarization and depolarization (i.e. short circuit) currents. However, for ferroelectrics, polarization currents are so large and hysteretic as to make this approach unreliable (Figure 4).

At elevated temperatures and voltages, current for $BaTiO_3$-based X7R devices decreases with time as

$$I = I_o t^{-m} \quad (4)$$

with exponent n varying weakly with voltage (Figure 5), and more strongly with temperature (Figure 6). Near room temperature, n is close to unity for these devices, decreasing roughly linearly with temperature at higher temperatures.

The current-time behavior of $BaTiO_3$-based Z5U devices is similar in form to that of X7R, as indicated in Figure 4. Exponent m values are near unity, decreasing with temperature, and relatively independent of voltage.

The agreement between measured polarization current and that estimated from equation 3 is indicated in Table 1.

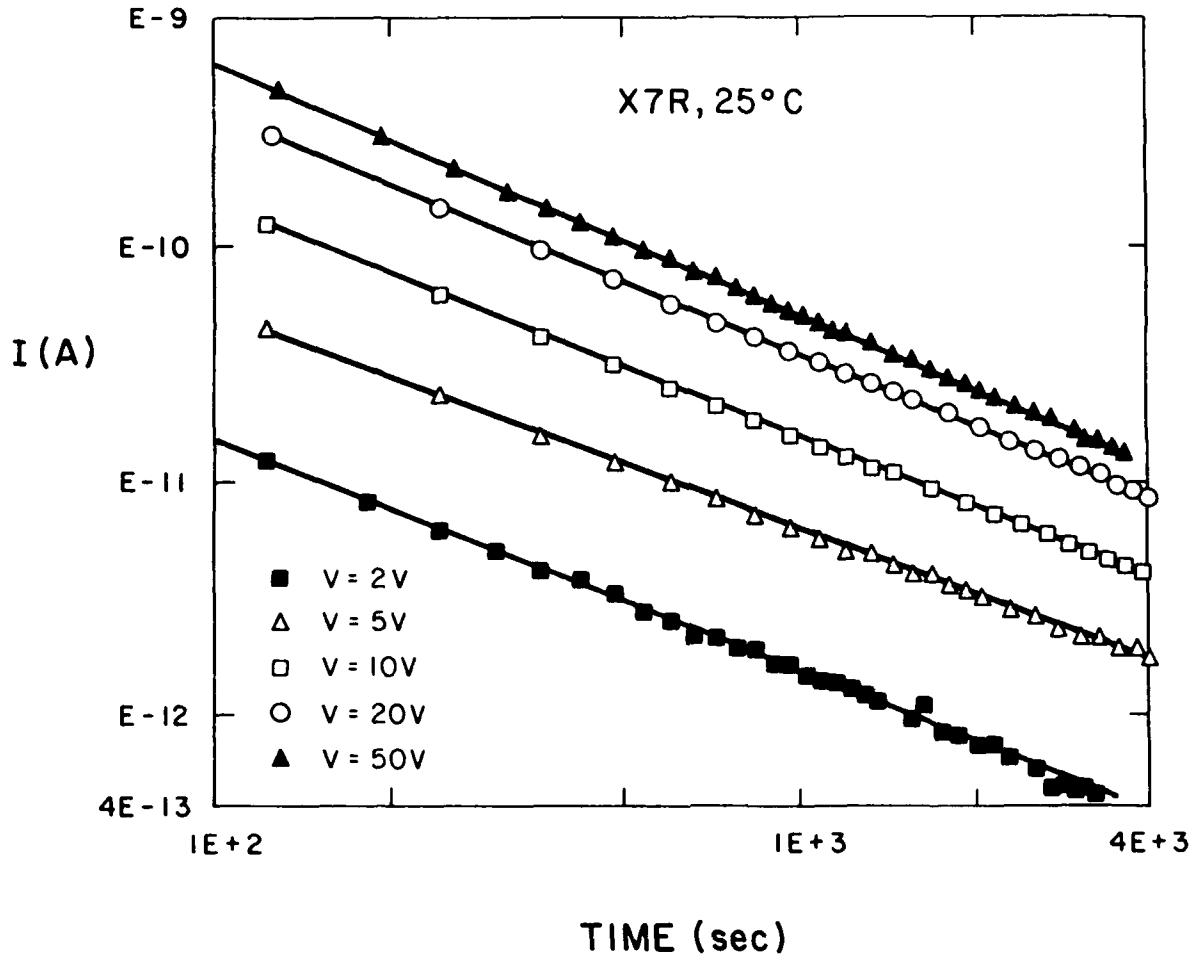

Figure 2. X7R leakage current after application of voltage, for five voltages. The decrease nearly follows an inverse time dependence at room temperature.

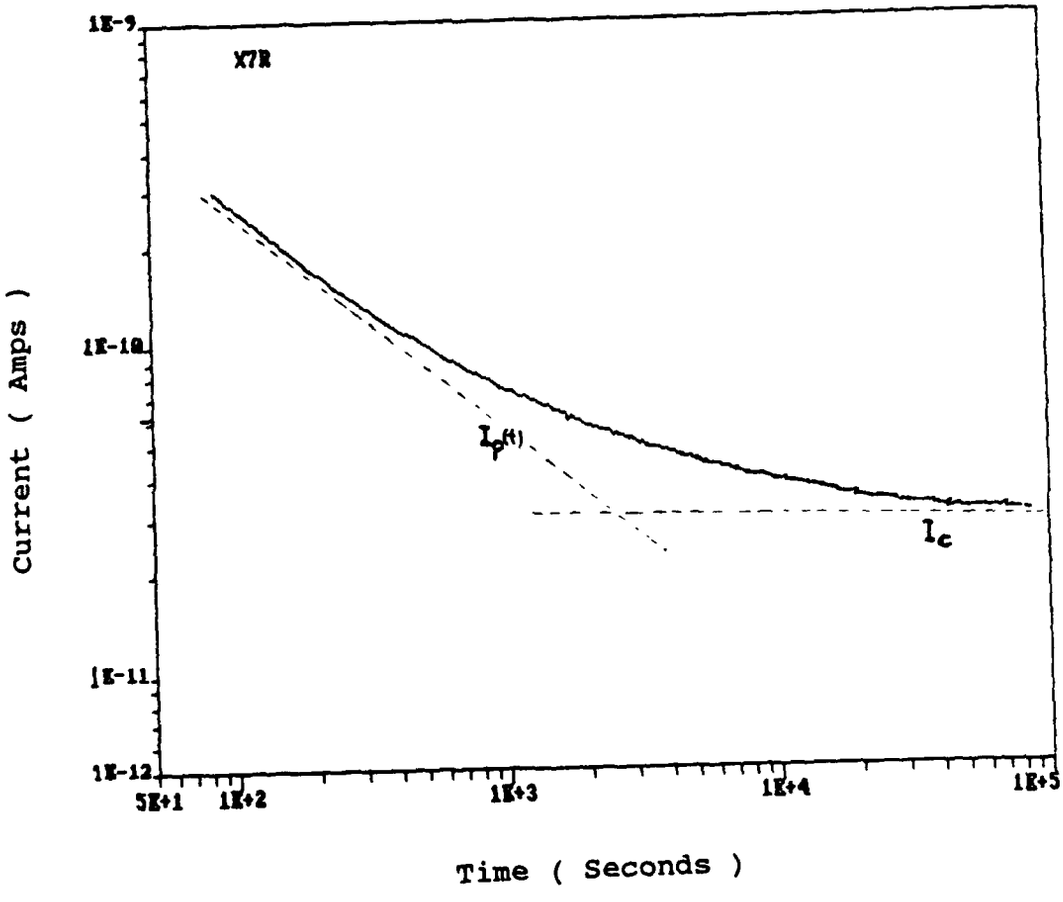

Figure 3. Transition from polarization current (I_p) to conduction current (I_c) for X7R at 100°C, 20V.

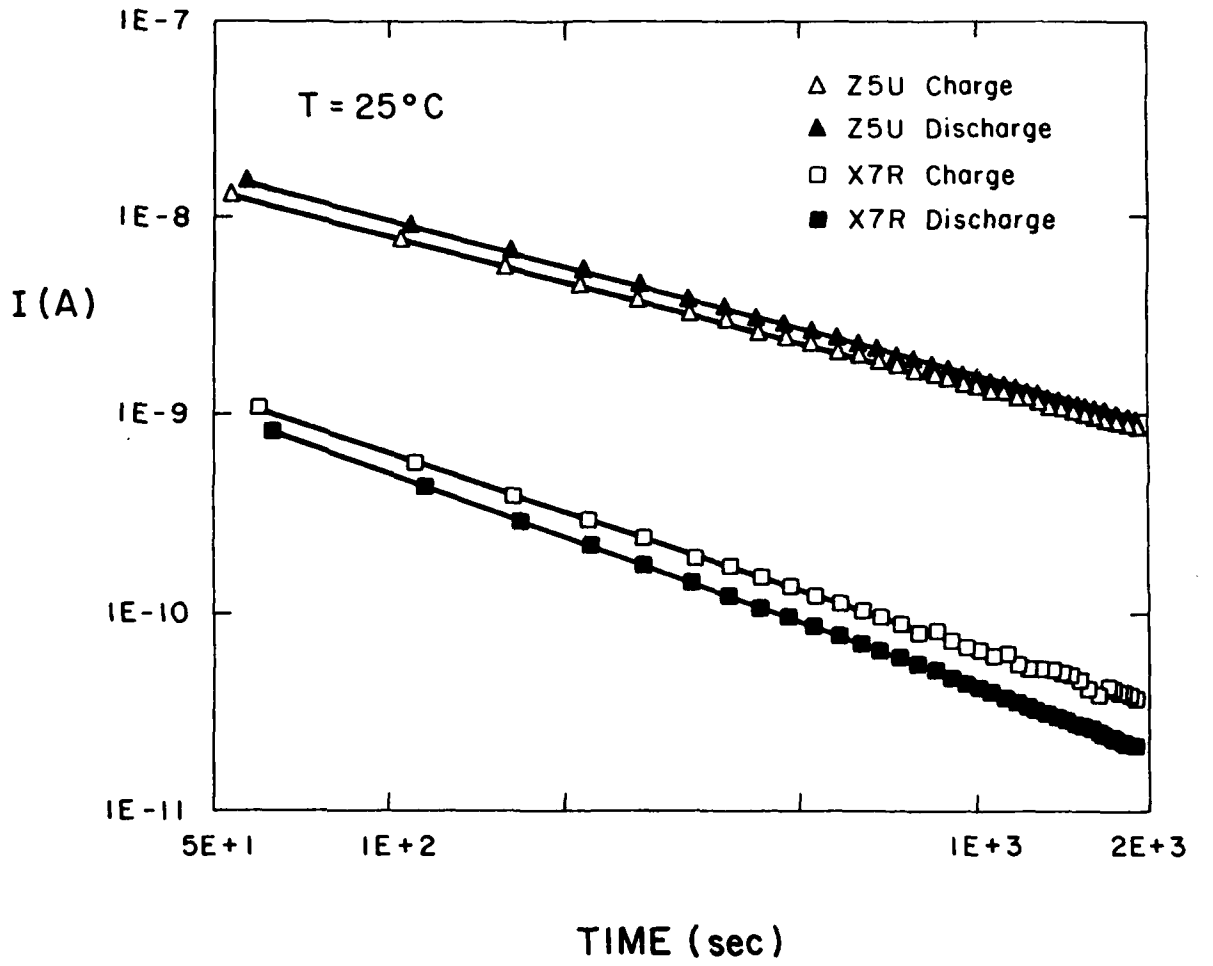

Figure 4. This figure illustrates two points: i) Equation 4 is satisfied by Z5U and X7R devices, although with different exponents; ii) Transport current cannot be deduced from polarization-depolarization currents.

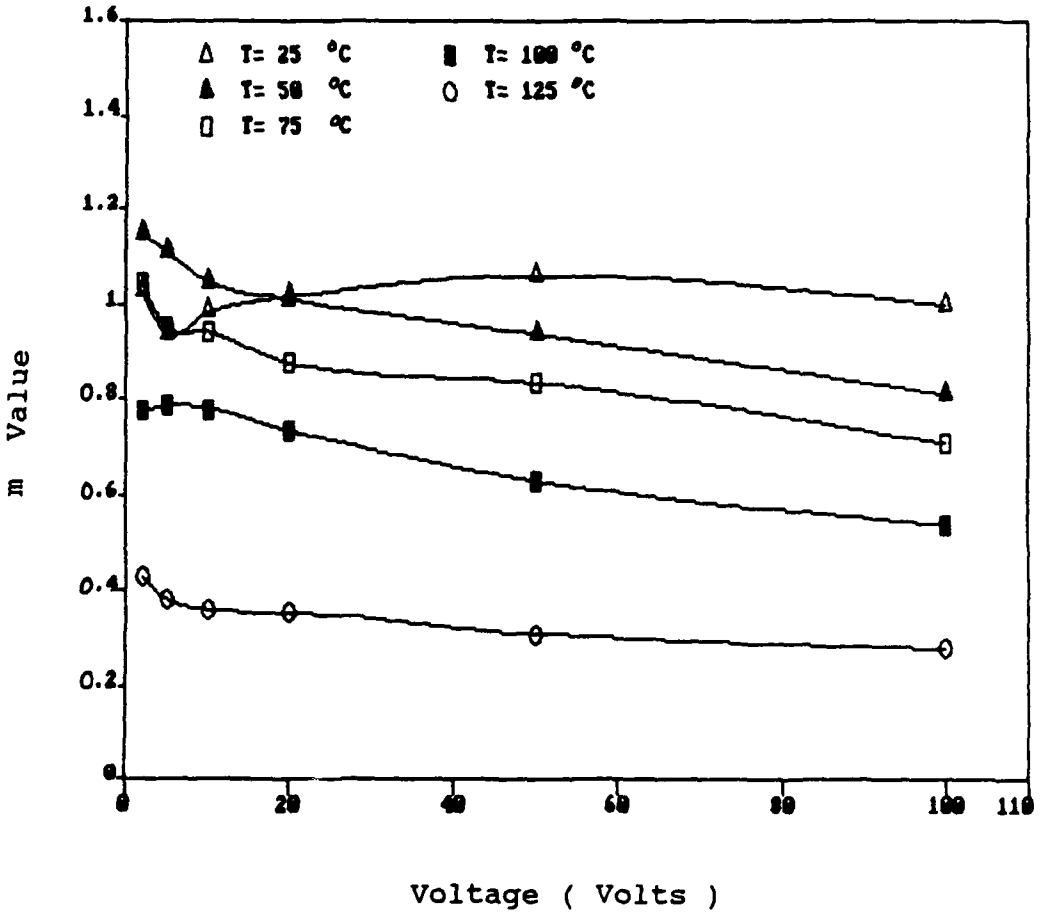

Figure 5. The exponent parameter m varies weakly with voltage (X7R shown; Z5U similar).

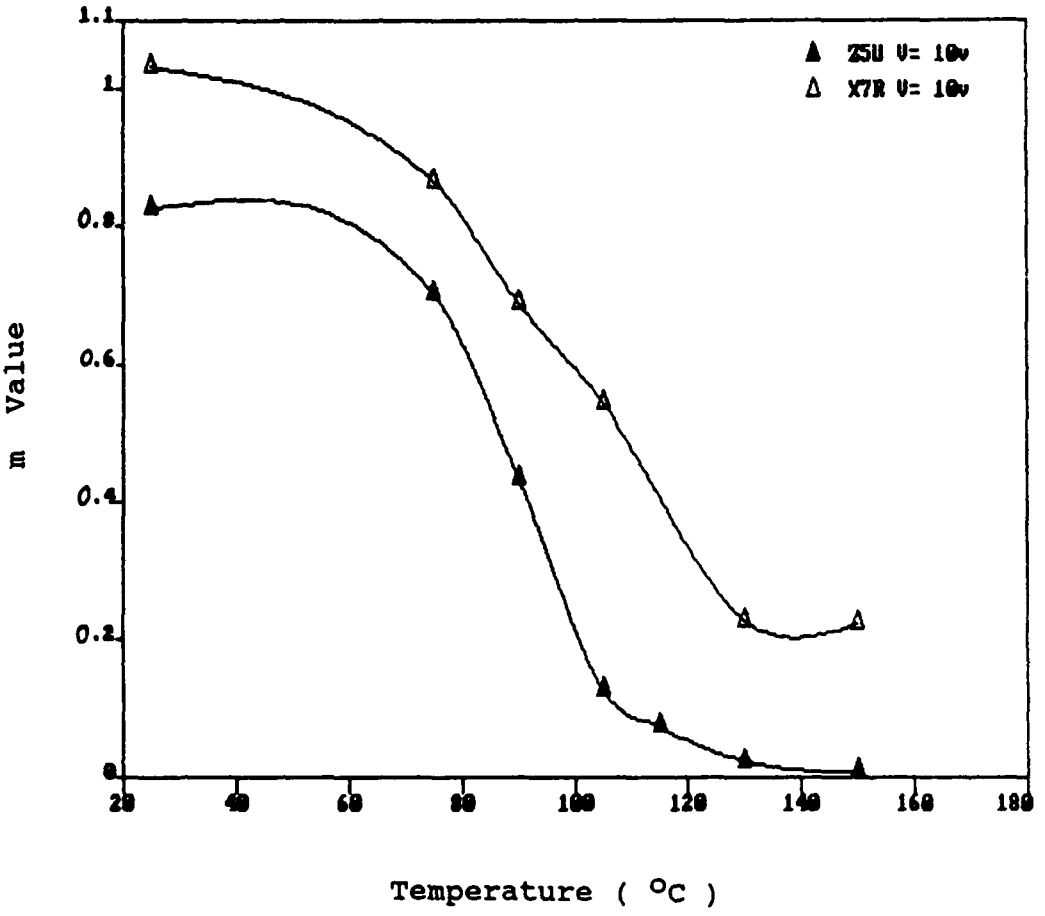

Figure 6. Exponent parameter m varies strongly with temperature for both X7R and Z5U.

Table 1

Comparison of measured currents and those deduced from the relation $I_p = C_1V/t$ (X7R at 100V, Z5U at 10V)

Type	C_1(F)	t(sec)	C_1V/t(A)	I_p(measured) (A)
X7R	$3x10^{-10}$	100	$3x10^{-10}$	$3x10^{-10}$
		500	$6x10^{-11}$	$5.6x10^{-11}$
		1000	$3x10^{-11}$	$2.8x10^{-11}$
		2000	$1.5x10^{-11}$	$1.4x10^{-11}$
Z5U	$2.84x10^{-8}$	100	$2.8x10^{-9}$	$2.9x10^{-9}$
		500	$5.7x10^{-10}$	$7x10^{-10}$
		1000	$2.8x10^{-10}$	$3x10^{-10}$
		2000	$1.4x10^{-10}$	$1.6x10^{-10}$

From these and similar results it is evident that for high resistance (i.e. un-degraded) ceramic, true leakage currents cannot be reliably measured at temperatures less than about 150°C unless one waits for times on the order of an hour or more, especially at lower voltages.

2.2 I-V-T Behavior

Useful information concerning charge carrier injection and transport, and degradation, can be discerned from dependence of leakage current on voltage and temperature. This has been discussed in detail in progress reports [1-3], journal articles [4-9], and references contained therein. The major types of DC current we have considered are summarized in Table 2 [1,4].

I-V characteristics were measured for new and degraded capacitors, mainly the X7R type. New devices were measured at elevated temperatures (≥130°C) so as to obtain stable currents; degraded devices could be measured at lower temperatures due to their larger transport currents.

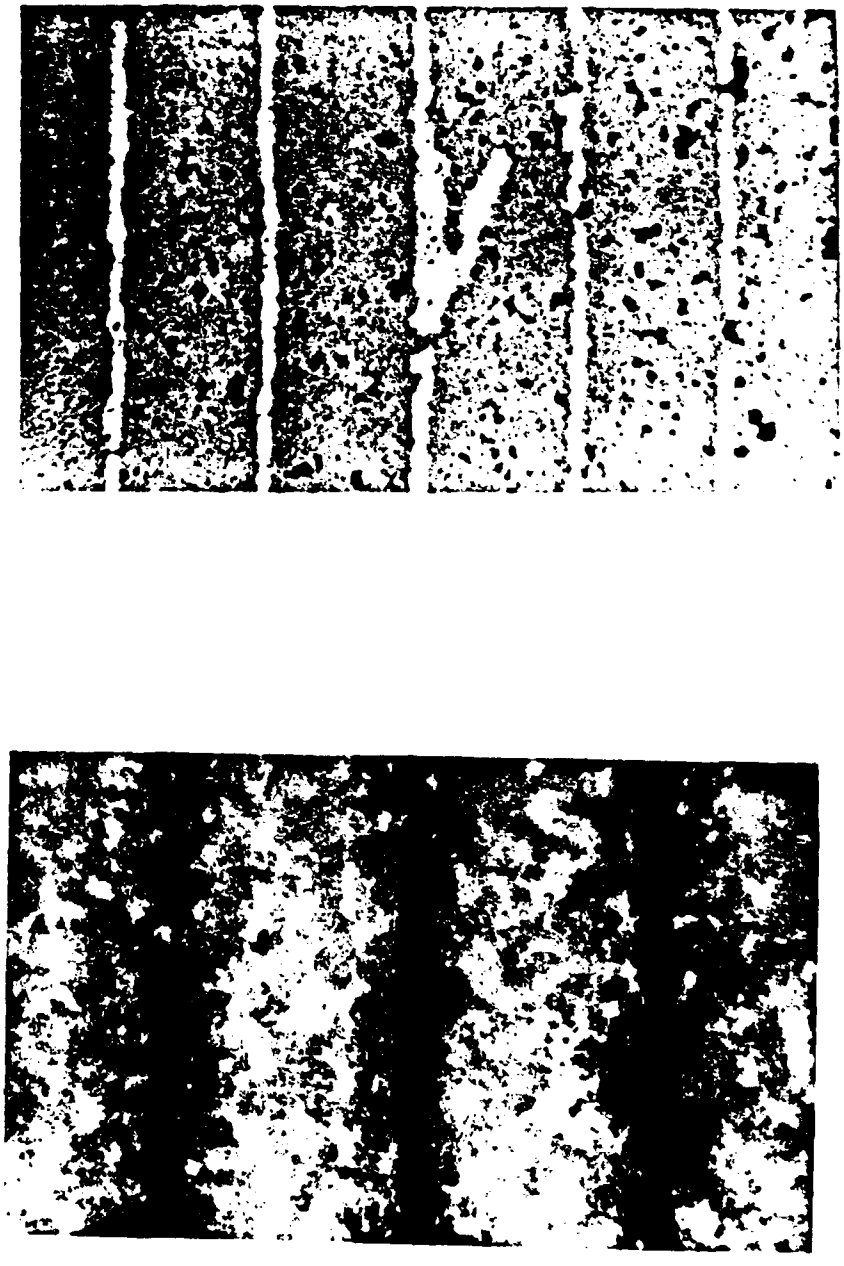

Figure 7. Asperities from X7R electrodes (top - 900X; bottom - 1400X).

Table 2

Voltage dependence of major current types

Type	Voltage Dependence
Ohmic	V
Space charge-planar electrodes	V^n, $n \simeq 2$
Space charge-point electrodes	$V^{3/2}$
Schottky	$\exp \sqrt{V}$

Several trends were apparent from these measurements. Ohmic behavior dominates at low voltage ($\leq$1V). At higher voltages, higher power voltage behavior invariably ensues, the most common type being at or near a $V^{3/2}$ dependence. For degraded devices, V^n behavior with $n \geq 2$ was evident, with hysteresis (discussed in more detail in next section.)

We presented a model for the $V^{3/2}$ current based on electron emission into the dielectric from hemispherical tips of electrode protuberances [1]. Another example of a somewhat similar nature that has been reported is electron emission from rough cathodes in MOS capacitors [10-12]. Cross sectioning of MLC devices indicates a large number of potential electron emitters, electrode asperities where the electric field will be enhanced due to metal curvature, and where the dielectric thickness is reduced. Examples are seen in Figure 7. The enhanced electric field that will exist at the tip of such an emitter must be viewed as a possible source of degradation, since both local joule heating (due to increased current density) and oxygen ion and vacancy diffusion (due to the larger field and perhaps temperature) will be enhanced. Such ion movement could account for the transition from 3/2 to quadratic voltage

dependence that occurs with degradation. This is discussed in that context in Section 3.

Thermal activation energies (Φ) were also of interest. For new devices and similar $BaTiO_3$ ceramic, values of 1.2-1.3eV are typical. There are several mechanisms to which such an activation energy for transport current may be attributed: oxygen ion diffusion [14], polaron hopping transport [15,16], grain boundary (GB) barrier transport [17,18], and activation of a deep donor. For reasons delineated in the following section, oxygen ion diffusion and deep donor activation are ruled out, leaving polaron and/or GB-dominated transport.

We discovered and reported two very striking properties of the thermal activation energies for MLC devices: they decrease markedly (eventually to zero) as devices degrade; they decrease with applied voltage for barrier layer and NPO types, although not for the X7R type from two vendors. The decrease of Φ with voltage is accompanied by superohmic current. Examples are seen in Figure 8.

Similar examples of voltage-dependent decreases in Φ, with accompanying increases in current, are well known for polycrystalline silicon [19] and ZnO varistors [20] (Fig. 8a). In such cases this is attributed totally to collapse of the GB potential barrier. Why this should occur for three of the device types shown in Fig. 8 and not for the fourth (X7R) is not clear. We have discussed the role of the GB in several publications [4-6,8,9]. The role of the GB with regard to electron transport is reviewed in Section 2.4.

2.3 Type of Carrier

MLC capacitor degradation is characterized by an increase in leakage current. Two key questions addressed in this contract were: what <u>is</u> the leakage current, and what causes it to increase with time? Over the course

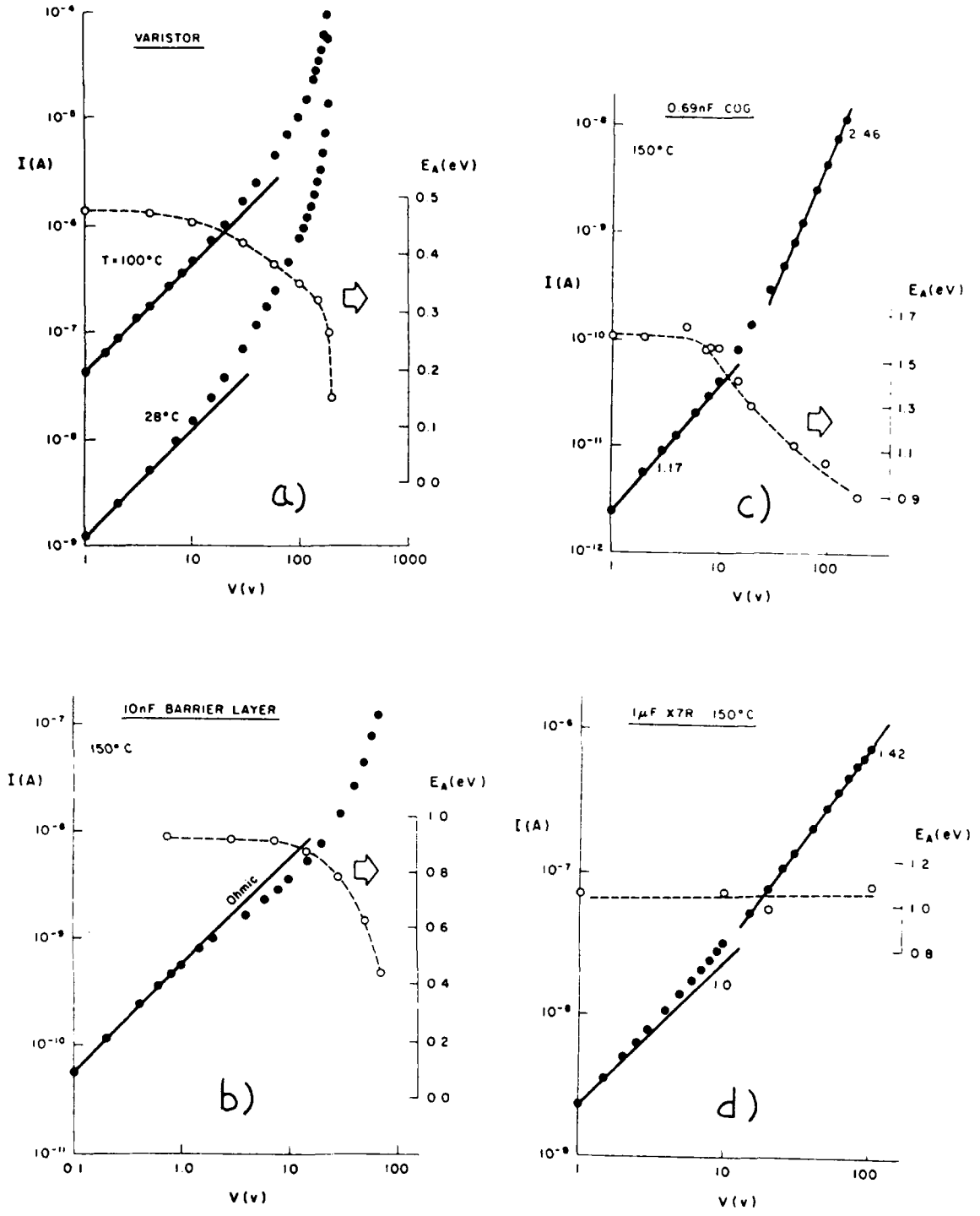

Figure 8. Current (I) and activation energy (E_A) dependence on voltage for a) varistor, b) barrier layer, c) COG and d) X7R devices.

of this program, we have measured mainly commercial capacitors, or similar "blanks", mostly $BaTiO_3$-based X7R. The results discussed below pertain to such samples. The nature of the charge carrier is discussed in this section; its increase with time (degradation) in Section 3.

Low-field electrical conductivity is proportional to carrier concentration and mobility. Possible carriers are ions, electrons and holes. In $BaTiO_3$-based material, conduction has been attributed to all of these. Certain carriers may predominate over given temperature ranges, or oxygen partial pressures.

We have verified that the dominant charge carrier in the type of X7R ceramic we have measured is the electron. (The fact that a majority of these electrons may originate from the movement of oxygen is discussed in Section 3.) This assertion is based on several pieces of evidence:

1) Leakage currents under accelerated conditions are constant with time, over extensive time periods. An example is shown in Figure 9, where current is seen to remain flat under different acceleration conditions over a time of nearly three months. If oxygen vacancies and conduction electrons are generated according to the relation

$$O_O \rightarrow \tfrac{1}{2}O_2 + V_O^{\cdot\cdot} + 2e' \qquad (5)$$

then it is not expected that leakage current would remain constant if vacancies and electrons (both conducting species) are generated by oxygen diffusion.

2) Negative Seebeck (thermoelectric) coefficients indicate that the charge carrier is negative [4]. Reproducibly negative and stable voltages generated verify that the charge carrier is negative, and of constant concentration over the time of the measurement.

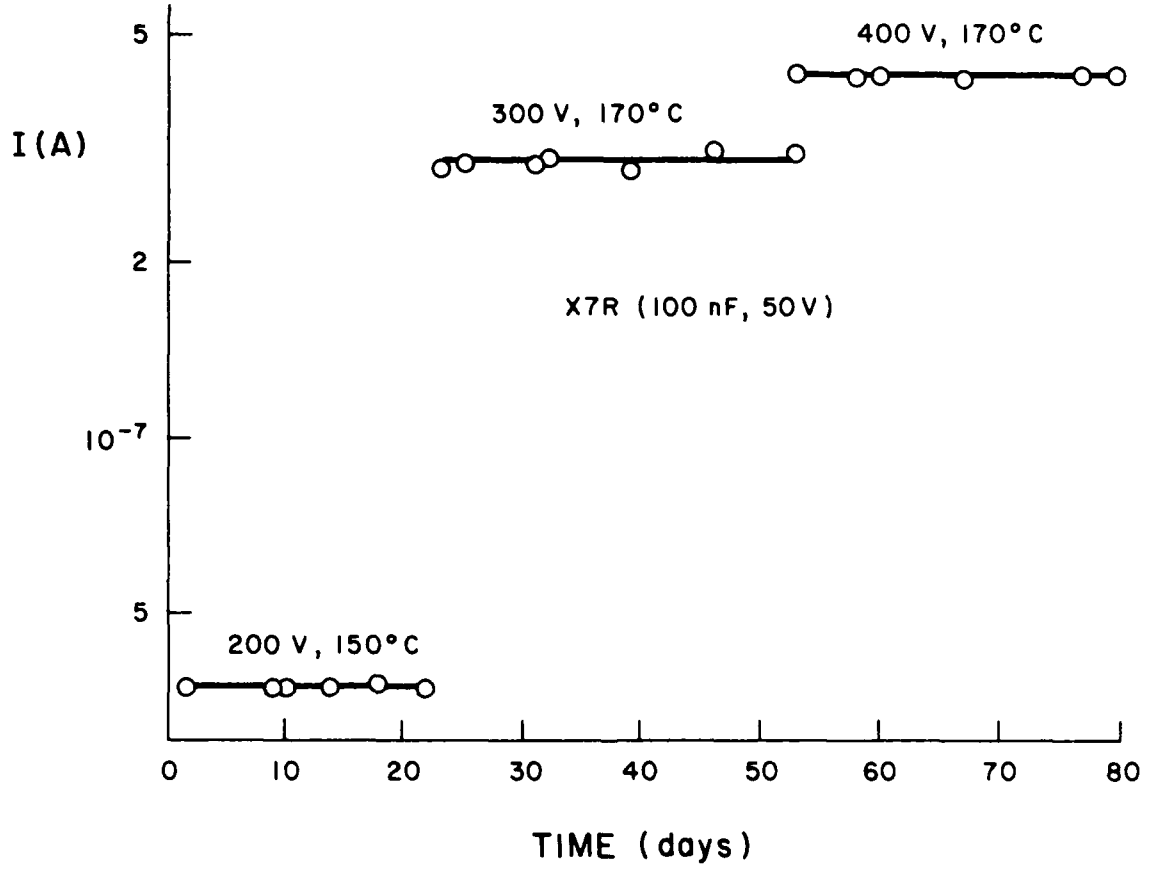

Figure 9. Leakage current versus time for an X7R under accelerated stress conditions, prior to degradation.

Seebeck measurements were also used to measure changes in carrier concentration and mobility for $BaTiO_3$-based X7R blanks reduced in hydrogen. Thermoelectric coefficient S versus temperature curves are shown in Figure 10a, for "new" and reduced samples. Carrier concentrations were deduced from the relation [21]

$$S = \frac{k}{q} \ln \frac{N}{n} \tag{6}$$

where $k/q = 8.63 \times 10^{-10}$ mV/K, and N and n are hopping site and charge carrier (polaron) concentrations respectively. Drift mobilities were determined from the relation $\sigma = nq\mu$, σ being measured simultaneously. Carrier concentration and mobility values are shown in Figures 10b and 10c. These are discussed more in Section 2.4.

3) Galvanic cell measurements on X7R blanks (supplied by Corning) indicate that, for this material over the temperature and oxygen pressures used, the charge carrier is not the oxygen ion. If there were considerable movement of oxygen and oxygen vacancies in $BaTiO_3$-based material (so as to make a contribution to conductivity, above the electronic contribution), this should be detectable as a Galvanic voltage.

The Galvanic setup and experimental results are shown in Figure 11, and were discussed in detail elsewhere [3,6]. We attempted to measure Galvanic voltages for six different $BaTiO_3$-based samples: two each of $Ba_{0.99}TiO_3$ and $Ba_{1.01}TiO_3$ (provided by MRL, Penn State), and two of the Corning X7R blanks mentioned earlier. A yttria modified zirconia (9.4M%Y_2O_3) disc was used as a known oxygen-ion conducting reference.

Experimental results are shown in Figure 11b. The Y_2O_3:ZrO_2 sample generates voltages slightly less than predicted by the equation

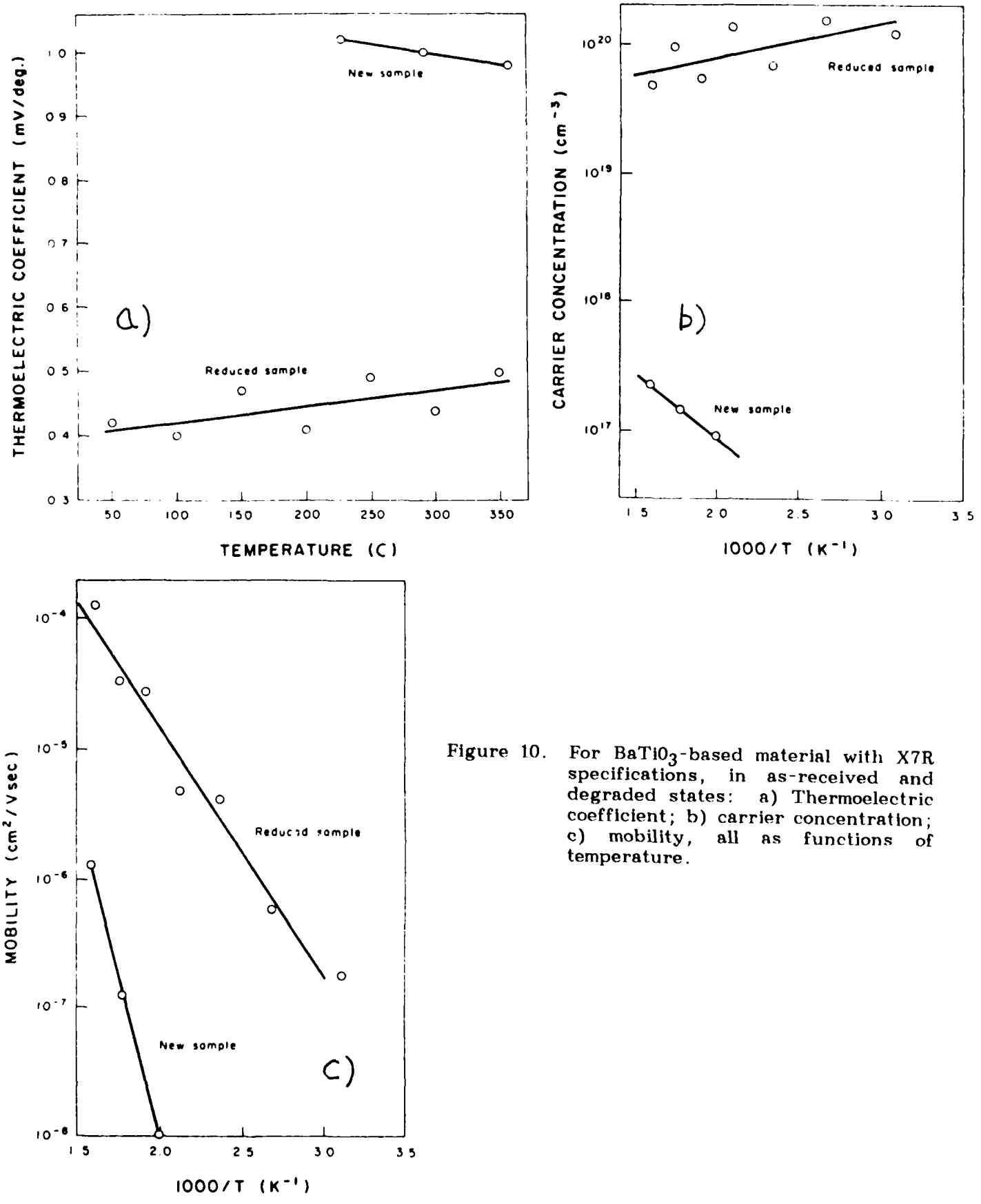

Figure 10. For $BaTiO_3$-based material with X7R specifications, in as-received and degraded states: a) Thermoelectric coefficient; b) carrier concentration; c) mobility, all as functions of temperature.

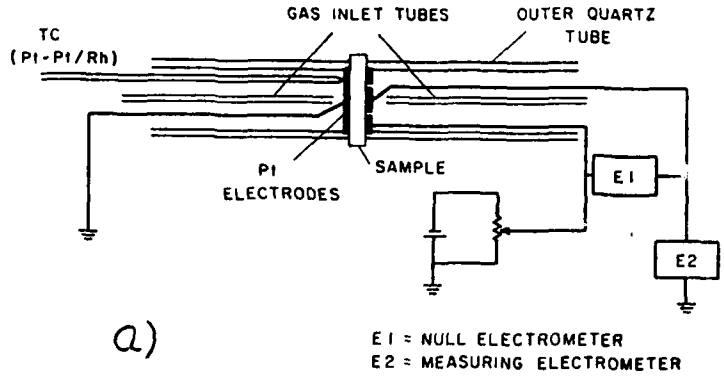

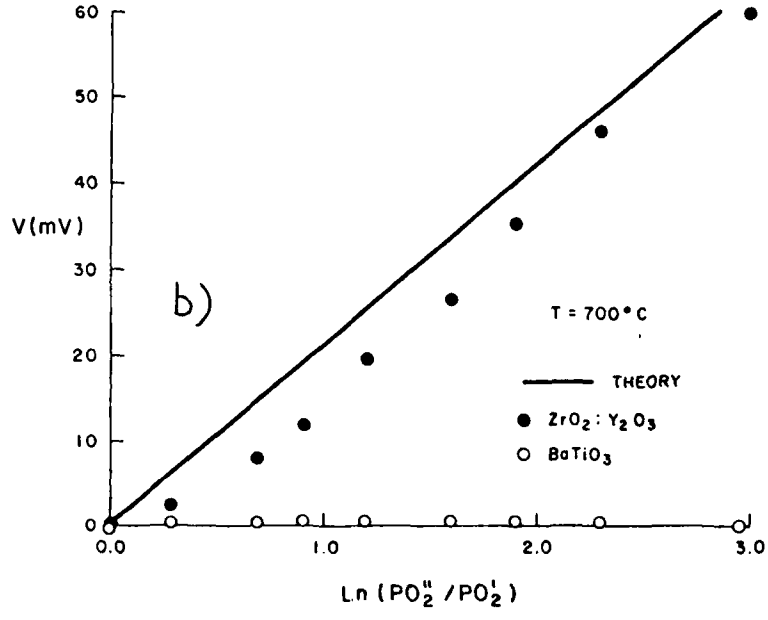

Figure 11. a) Galvanic cell setup, and b) Galvanic voltages for $ZrO_2:Y_2O_3$ and $BaTiO_3$-based discs.

$$V = \frac{RT}{4F} \ln \frac{P''(O_2)}{P'(O_2)} \qquad (7)$$

which is the solid line of Figure 11b. These voltages may be slightly low because the temperature (700°C) is somewhat low for ZrO_2 [22].

All of the $BaTiO_3$-based samples generated essentially zero voltage at all temperatures and oxygen pressures used. This indicates that oxygen diffusion is not significant in these samples over 500-700°C, and is therefore probably not significant at lower temperatures. Thus it appears that the exponential increase in conductivity with temperature seen for such samples is not due to enhanced diffusion of oxygen or oxygen vacancies (even though such diffusion may be responsible for degradation or a conductivity increase with time, as discussed below.)

4) We have reported [1,4], and there have been many other reports [23-26], of space charge limited currents in $BaTiO_3$-based materials and capacitors. Thus, even though ionic SCLC can potentially exist, and has been reported in other materials [27], we do not feel that the SCLC reported for $BaTiO_3$ is ionic because there would have to be a steady supply of ions supplied by an electrode (cathode for $O^=$) for a constant current to exist over many days or even months. The SCLC is due to electrons injected from the cathode.

The above four points seem to verify that the charge carrier forming the leakage current, for the $BaTiO_3$-based samples we have measured, is the electron.

2.4 Carrier Transport

We attempted early in the program to directly measure carrier mobility μ using the conventional van der Pauw to technique [1]. These results were

unsuccessful, i.e., no Hall emf could be measured even at elevated temperatures. The mobility sensitivity of our setup was about $0.01 cm^2/Vsec$. Other measurements (Seebeck and estimates from SCLC characteristics) confirm that μ values for such ceramic were much less than $0.01 cm^2/Vsec$.

For undegraded (un-reduced) samples, mobilities were determined to be less than about $10^{-6} cm^2/Vsec$. This is consistent with a small polaron hopping mechanism for electron conduction [16], although the values are much less than those reported by Seuter [26].

The conductivity σ can be expressed as

$$\sigma = qn\mu \qquad \mu_o e^{-\Phi_n/kT_e} e^{-\Phi_\mu/kT} \tag{8}$$

where Φ_n and Φ_μ are carrier concentration and mobility activation energies.

Thermal activation energies deduced from figures 10 and 11 for X7R blanks are shown in Table 3.

Table 3

Thermal Activation Energies (eV)

Sample	Concentration	Mobility	Carrier Conductivity
New	0.19	1.03	1.22
Reduced	~0	0.34	0.34

The conductivity activation energy is ~1.2eV for as received X7R chips, which is close to that of a new X7R capacitor from the same vendor (Corning.) The decrease in activation energy of the reduced chip (0.34eV) also corresponds to the similar decrease we have measured for degraded capacitors (discussed in Sec. 3.)

The temperature dependence of electron transport in these materials resides almost entirely in the mobility. The weaker temperature dependence of carrier concentration indicates near-complete ionization of donors.

This is consistent with polaron hopping transport of electrons. The total electron concentration is essentially constant; the electrons must overcome a potential barrier, which would be the Φ_μ of equation 8 [38].

The possibility of transport being dominated by grain boundaries (GB) was treated in some detail, for two major reasons: 1) It is know that GB control transport in certain other polycrystalline materials, namely thin films [29], polycrystalline silicon [19], barrier layer capacitors [30], ZnO varistors [20], and $BaTiO_3$ thermistors [17]. 2) The voltage dependent activation energy that we reported for COG capacitors (although not for X7R.)

Several types of GB potentials are shown in Figure 12, for homogeneous and inhomogeneous grains. Currents that can flow across a GB are also illustrated in Figure 12. For Schottky barrier type electron emission over the GB barrier (with no voltage drop in the grain), the I-V relation is

$$I = I_o e^{-\Phi_B/kT}(e^{qV/kT} - 1) \tag{9}$$

where Φ_B is the GB barrier height. At a given voltage this expression can be approximated by

$$I = I_A e^{-E_A/kT} \tag{10}$$

where E_A is an activation energy approximately equal to Φ_B. If conduction is dominated by electron mobility μ, the latter can be expressed

$$\mu = \mu_o e^{-\Phi_B/kT} \tag{11}$$

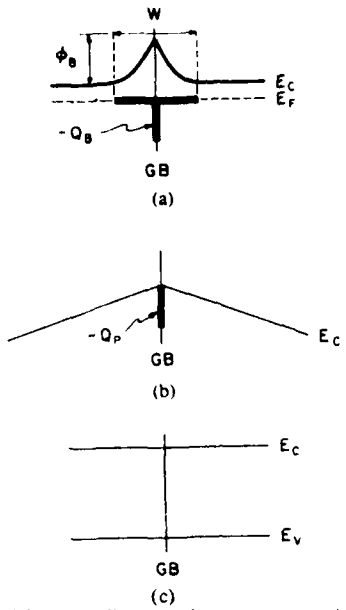

a) GB potential energy diagrams, homogeneous grains. (a) Negative charge trapped at GB. $\Delta P_s = 0$; $Q_{GB} = qN_{GB}$. (b) Normal polarization discontinuity. $\Delta P_s = Q_P$; $N_{GB} = 0$. (c) Reduced poly-Si, no charge at or near GB (flat bands). $\Delta P_s = N_{GB} = 0$.

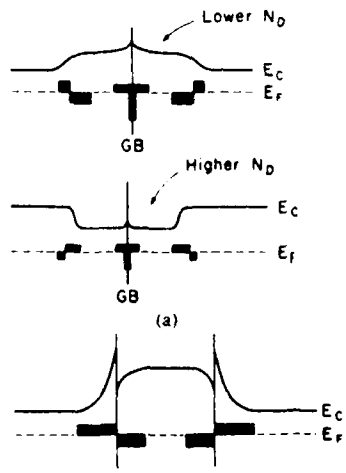

b) GB band diagrams, inhomogeneous grains. (a) High-resistance layer near GB. (b) Low-resistance layer. (c) Presence of second material or phase.

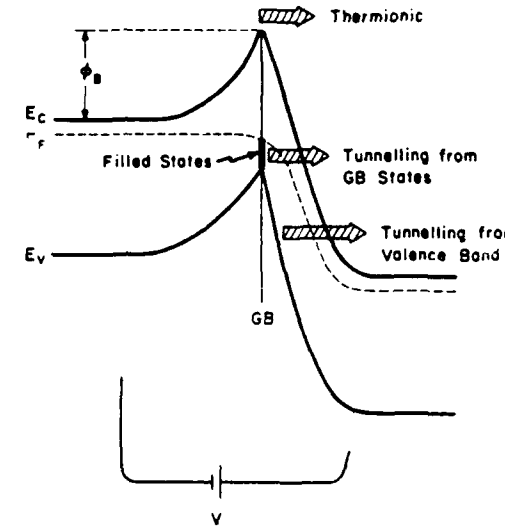

c) Grain boundary under bias, for low-resistance grain (i.e., $V = V_{GB}$).

Figure 12. Grain boundary potential energy diagrams for a) homogeneous grains; b) inhomogeneous grains. c) Illustration of current types in the vacinity of a GB.

Highly super-ohmic I-V behavior is accompanied by decreasing activation energy (Figures 8a, 8b, 8c for varistor, GBBL capacitor and COG capacitor, respectively). The weaker superohmic behavior of $BaTiO_3$-based X7R devices ($\sim V^{1.5}$) is not accompanied by a decrease in Φ (Fig. 8d) We reviewed the theory of GB transport, and voltage dependent GB impedance [5]. One complication for high resistance capacitor ceramic is the high grain resistance (unlike the GBBL material, or any of the others mentioned earlier). Even so, if a fraction of the applied voltage is dropped across the GB, its potential barrier should eventually collapse, resulting in superohmic current.

Therefore, the question to be addressed was: How is GB impedance measured? One approach is to place micro-probes directly across a GB. This is feasible for large grained material, especially if grain resistance is small. However for smaller grained X7R material, with high grain resistance, the problems of small size and surface conductance arise. A second approach, which we pursued, is that of complex impedance measurements of the type originally reported by Baurle [31]. The reader is referred to the references for details [3,9,31].

In summary, if the impedance contributions of a given solid can be represented by lumped R-C sections, these can be discerned on a complex impedance plot if the RC time constants are distinct. The complex impedance Z is defined as

$$Z = Z' + j\,Z'' \tag{12}$$

where Z′ and Z″ are resistance and (capacitive) reactance respectively, which are both functions of frequency and the R-C elements representing the solid.

For our X7R samples, the only possible RC contributions were assumed to be from the GB and grains, since resistivity was not a monotonic function of sample thickness, thus eliminating contact resistance (see Table 4)

Table 4

Resistivities for X7R Chips of Different Thickness

Chip Thickness (mm)	Resistivity (Ω-cm)
0.14	1.59×10^6
0.21	2.31
0.41	1.77
0.41	1.92
0.69	1.90
1.12	2.17

An impedance plot (Z'' vs Z') is shown in Figure 13a for a commercial varistor, across the frequency range 5Hz - 13MHz, under different voltage biases. Only one semicircle is evident at a given bias because only the GB contributes significantly to impedance; the circle radius reduces with voltage because of GB collapse.

Many impedance plots were made for $BaTiO_3$-based samples; all showed evidence of more than one impedance contribution, and none exhibited a single semicircular structure. An example is shown in Figure 13b, at bias voltages of zero, 50V and 100V. Two overlapping semicircles were always evident for Corning X7R samples of this type. The semicircles are offset upward from the real axis (centers indicated by crosses), this effect attributed to local inhomogeneity and dispersion. As pointed out by Kleitz et al. [32], the offset is usually small for intragrain semicircles (i.e. the grain contribution.)

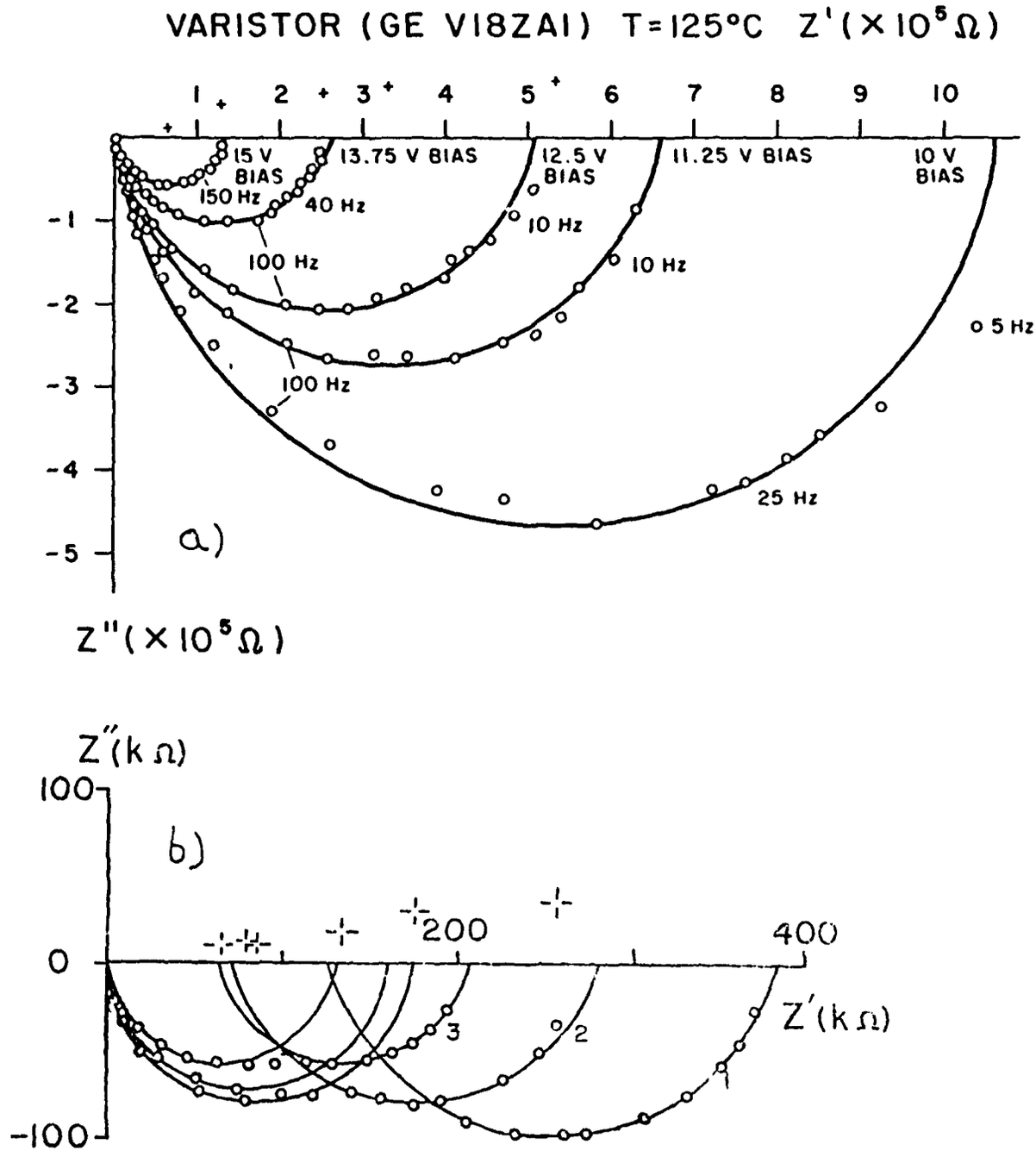

Figure 13. Complex impedance plots for a) commercial varistor, and b) X7R ceramic, at different voltage biases. The key for the X7R is: #1, zero bias; #2, 50V bias; #3, 100V bias.

We assigned the high frequency semicircles (left side) to the grains, and the lower frequency ones to GB. Resistance values obtained from this data are shown in Table 5, for different biases, for three samples. It is seen that the GB contribution decreases slightly more with voltage, which was generally the case for all samples measured. The ratios increase with voltage bias from two percent to 35 percent, which is significant. Such changes with voltage are consistent with superohmic I-V behavior which is controlled mostly by the GB.

Table 5

R_G/R_{GB} Versus Bias Voltage

Bias Voltage (V)	R_G/R_{GB} 1	2	3
0	0.58	0.65	0.46
10	0.73	0.71	0.51
20	0.70		0.51
35	0.74	0.69	
50		0.72	0.51
100		0.88	0.61
150			0.47

We also reported how grain size could be an important parameter with respect to GB impedance. GB barrier heights were computed versus grain diameter, and also versus grain carrier concentration [9,33]. Results are shown in Figures 14 and 15. Several things are apparent from this analysis, related to how GB can influence ceramic impedance:

1) Barrier height Φ can vary over orders of magnitude, from dominating (>1eV) to non-important, depending on grain size and donor density;

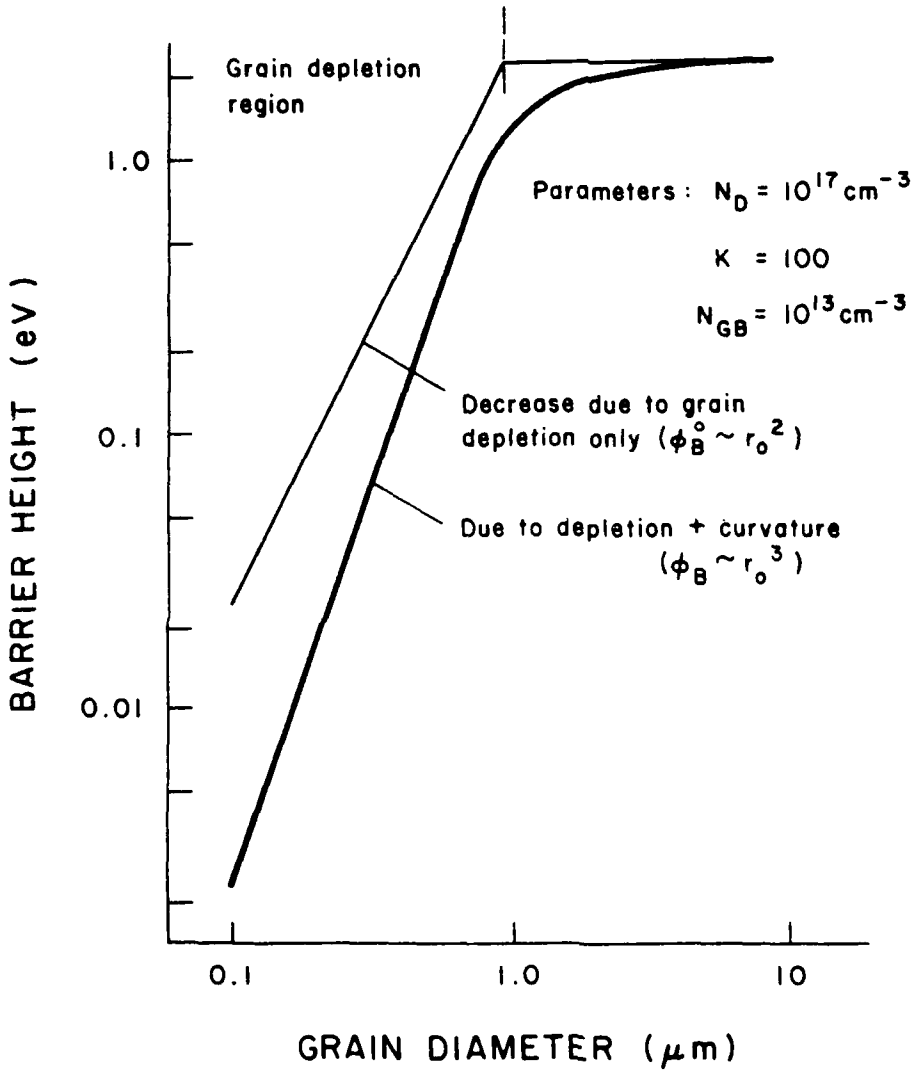

Figure 14. Dependence of GB barrier height on grain diameter for two cases: due to grain depletion only; due to grain depletion plus curvature. Other parameters are indicated in figure.

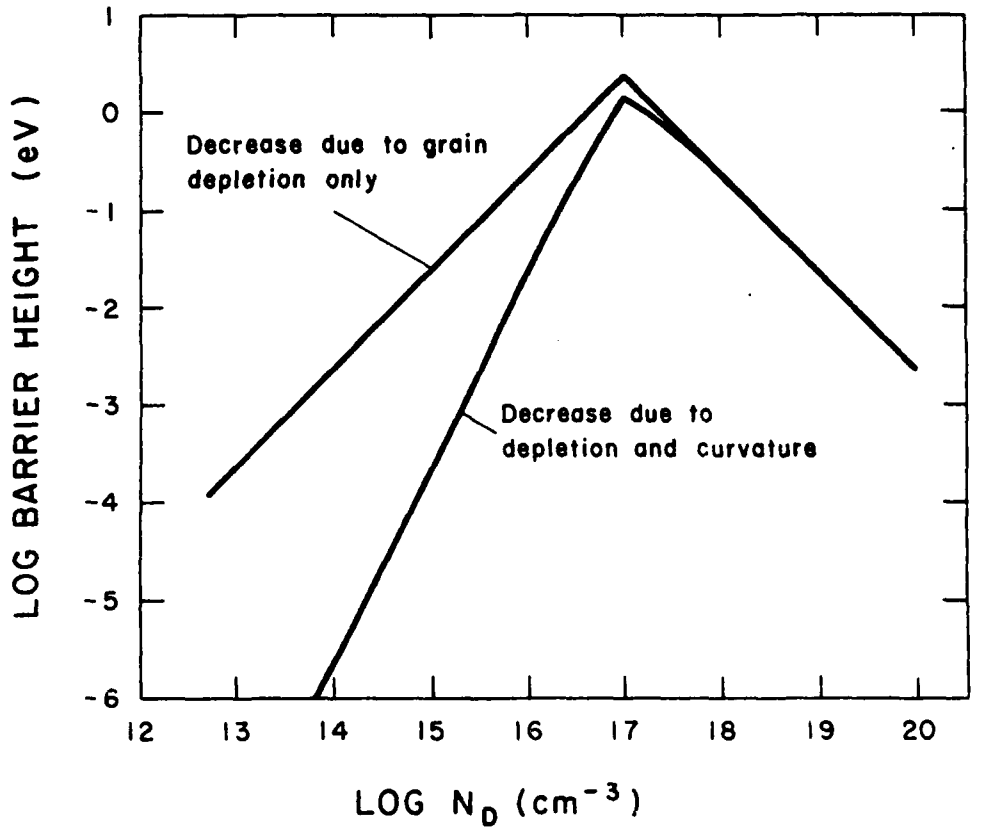

Figure 15. Dependence of GB barrier height on donor density in the grain for the same two cases as in Figure 14. The GB barrier height peaks at about $10^{17}cm^{-3}$.

2) Grain curvature can cause a substantial decrease in Φ for small grains;

3) Resistance homogeneity throughout the material could depend on grain size variation, with higher curvature grains offering reduced resistance paths;

4) Grain size variation could render a lumped RC model for the GB inappropriate; a distributed model would be neces-ary, and a "distributed" impedance plot could result. This could also account for some of the impedance plot offsets which we measured.

Thus, even though these results seem to shed some light on the role of GB in high-K ceramic, their exact role in both carrier transport and degradation is still unclear for the X7R type, the main one we measured. There is evidence of both grain and GB resistance contributions from the impedance plots. However, other results that we found call this interpretation into question; namely the following:

1) Single crystal and ceramic $BaTiO_3$ have similar activation energies E_A, of about 1.2-1.3eV;

2) The two apparent semicircles of our impedance plots have similar activation energies of about 1.3eV [39];

3) For X7R ceramic and devices, E_A values are essentially independent of voltage. For GB- controlled devices, this should not be the case.

4) $BaTiO_3$-based ceramic resistance has been reported to be independent of grain size, other parameters remaining constant [40].

3. INTRINSIC DEGRADATION

Most of our degradation measurements were made on commercial $BaTiO_3$ based Z5U and X7R capacitors, under accelerated voltage and temperature conditions. Other pieces of similar material, without internal electrodes, were also studied. Sections 3.1-3.3 review certain electrical characteristics for

degraded as compared to "virgin" samples. Section 3.3 discusses models which can account for these characteristics.

3.1 Time-Dependence

By far the most common type of time dependence seen for degradation was exponential, usually following some initial time period (typically several minutes.) Degradation characteristics for X7R devices are shown in Figs. 16 and 17. After an initial period, current varies exponentially with time until breakdown. This initial transition time t_o decreased with temperature for measured X7R devices as

$$t_o = (4x10^4 - 1.5x10^2 T) \text{ sec} \tag{13}$$

between about 200°C and 280°C.

Under lower stress, leakage currents remain constant over long time periods (Fig. 9). We have also reported the exponential increase for thick film capacitors [34]. Z5U devices follow a similar time behavior (Figure 18). Thus, the current-time relation for capacitor ceramic can be represented generically as shown in Fig. 19, where the time scale depends on voltage, temperature, and type of ceramic. The initial decrease in current was discussed earlier (Sec. 2.1).

Such capacitor degradation has been reported previously by Prokopowicz and Vaska [35], and by Minford [36]. Relative mean lifetimes were described in accordance with the empirical equation

$$\frac{\tau_1}{\tau_2} = \left(\frac{V_2}{V_1}\right)^n \exp\left[\frac{E_a}{k}\left(\frac{1}{T_1} - \frac{1}{T_2}\right)\right] \tag{14}$$

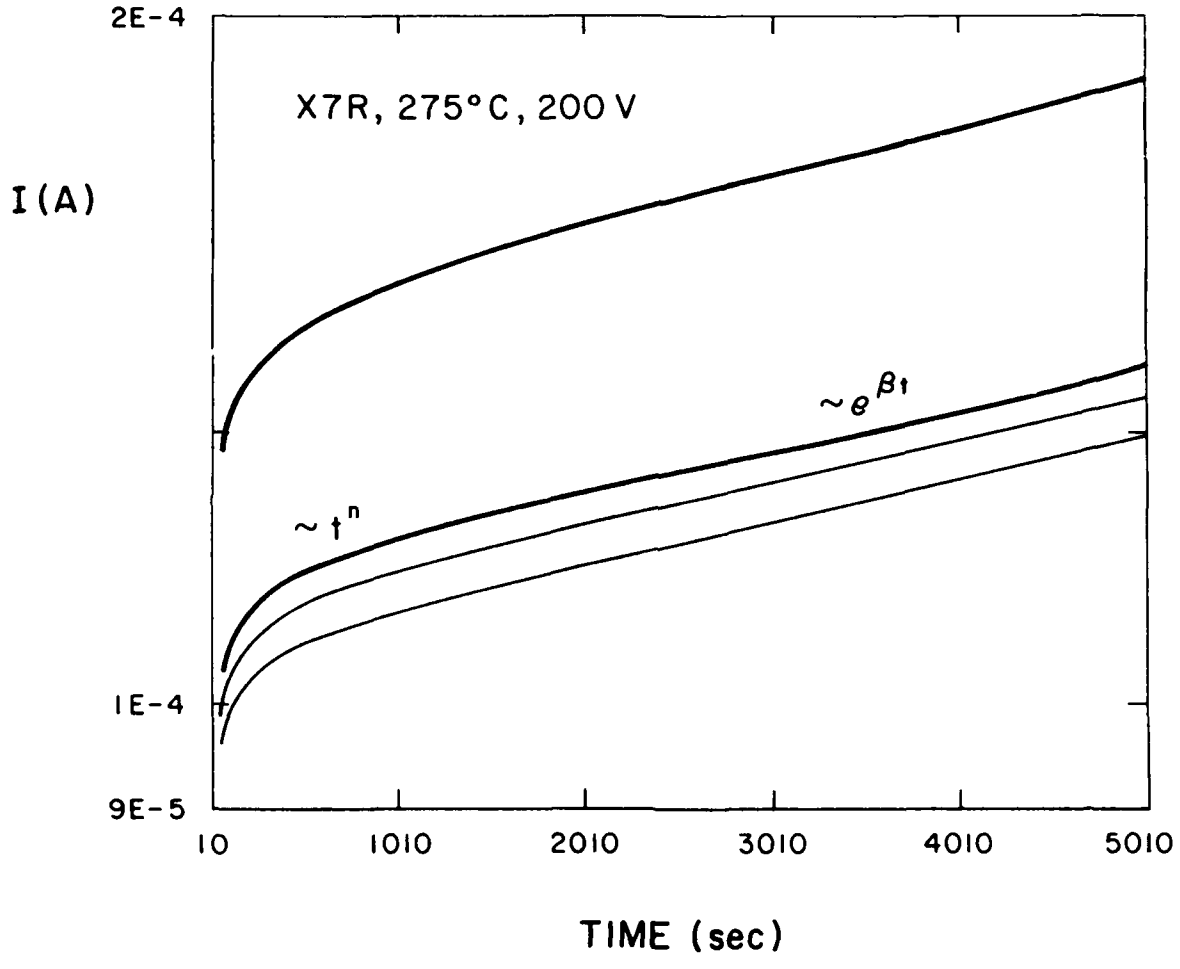

Figure 16. Degradation curves for four similar X7R devices. Currents initially follow a power law, and later exponential, time dependence.

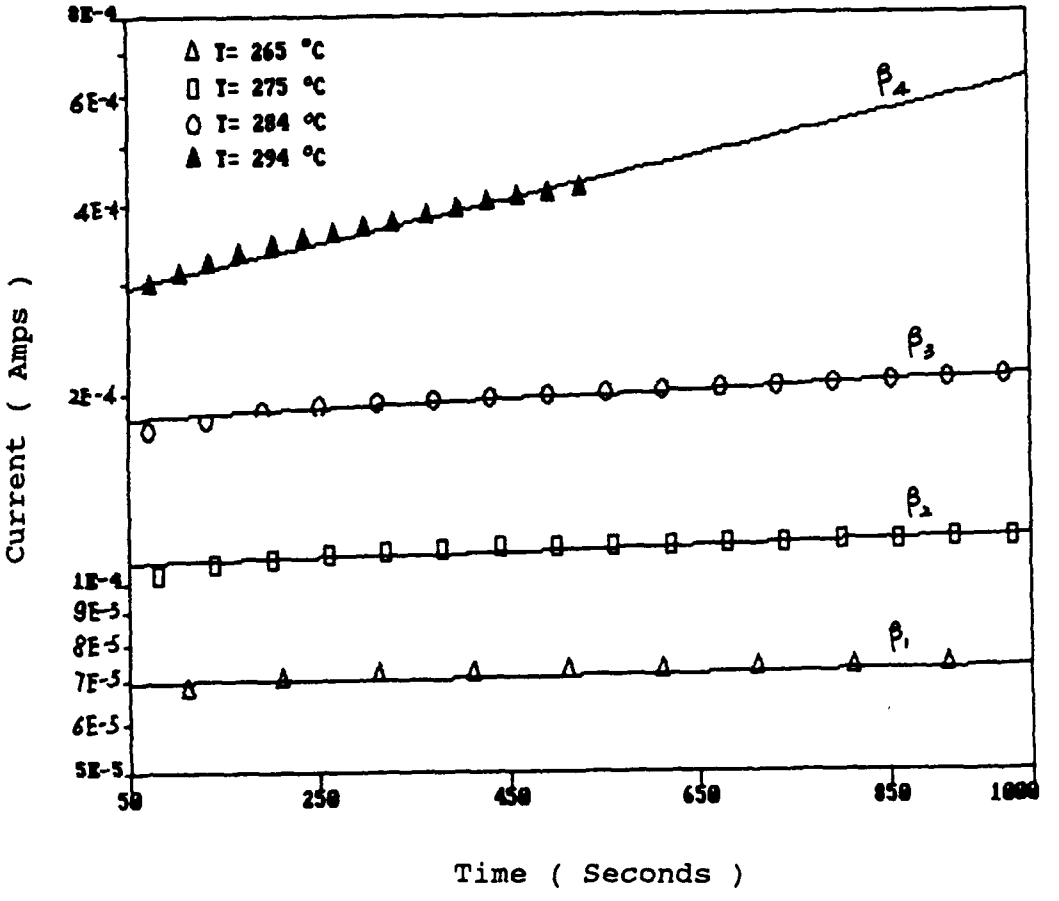

Figure 17. Degradation curves for X7R devices at four temperatures. Degradation rate parameter β was determined from least squares fits to such curves. For these, the β values are ($x10^{-5}$) : β_1=2.73; β_2=4.32; β_3 =6.91; β_4=34.7.

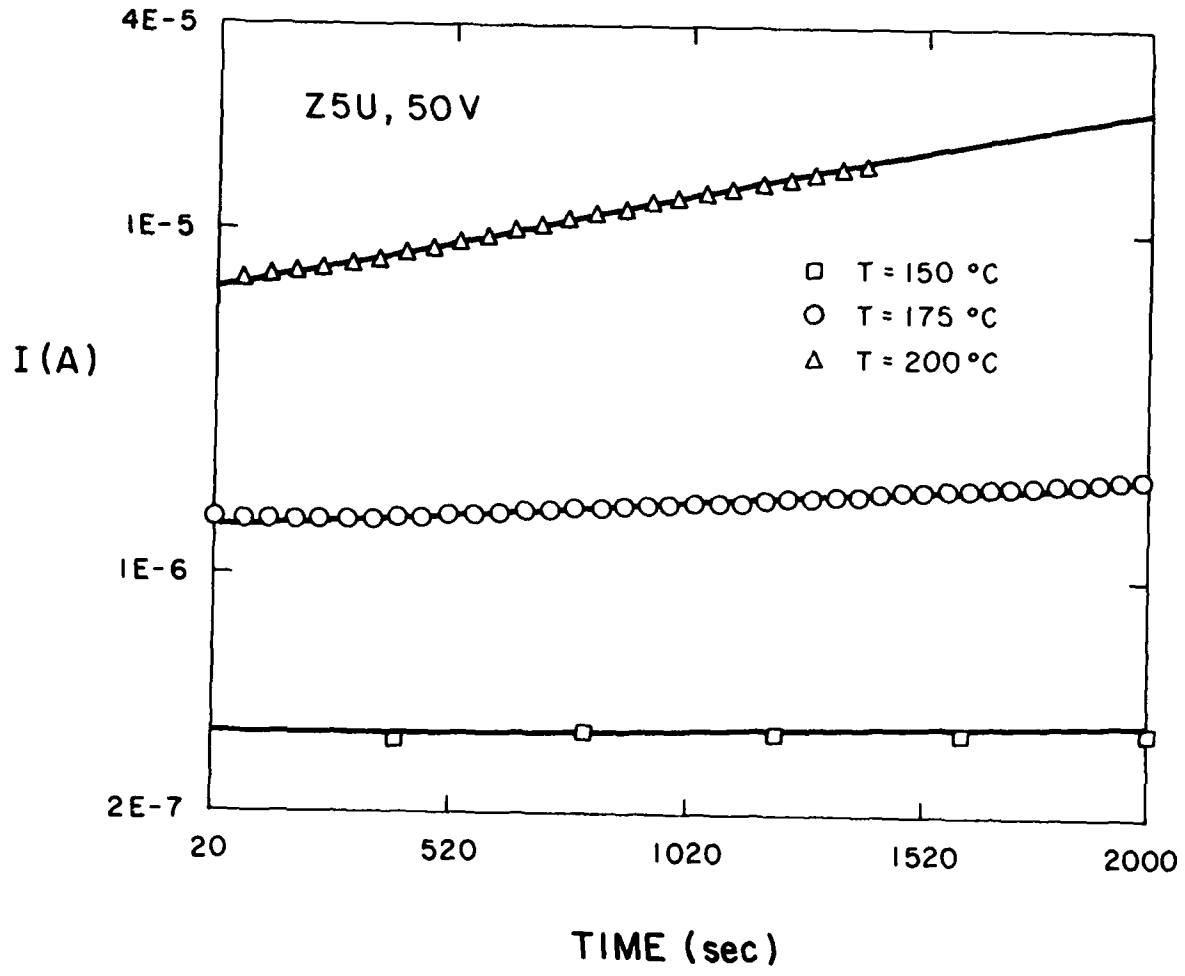

Figure 18. Degradation curves for Z5U devices at three temperatures.

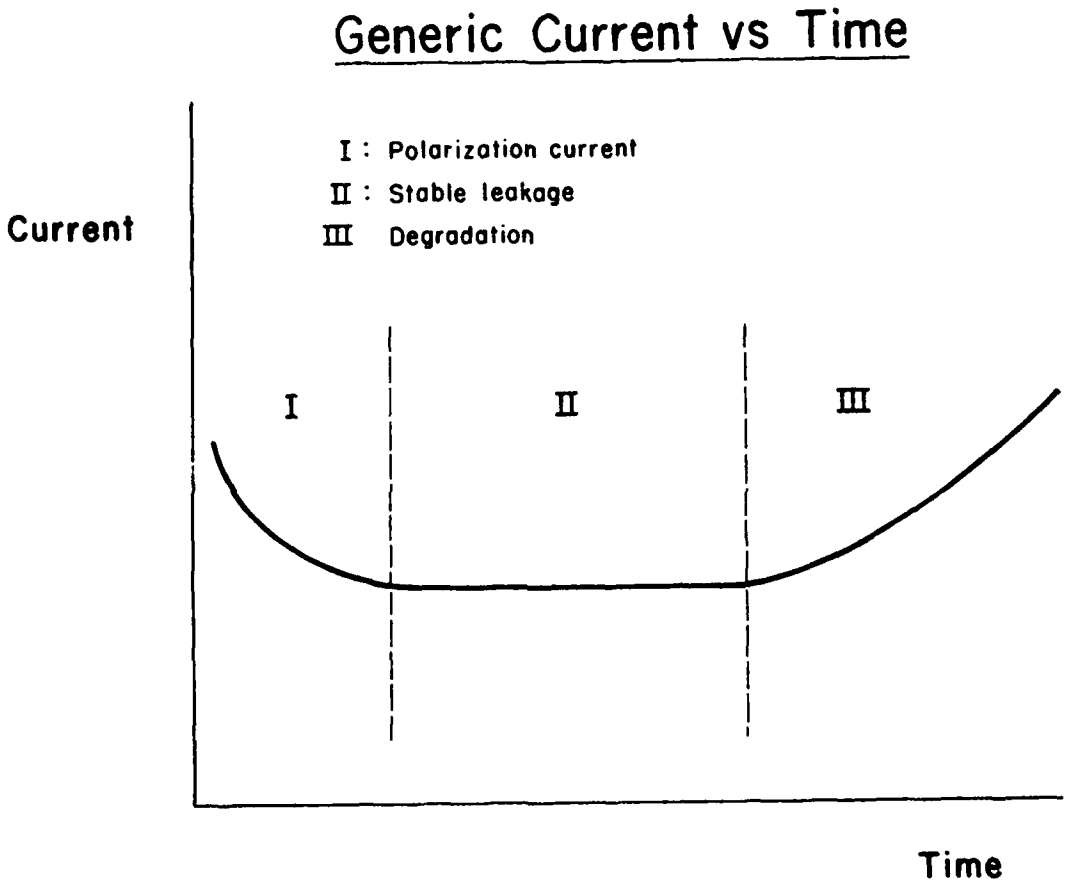

Figure 19. Generic current-time curve for dielectrics.

where τ_1 and τ_2 are device lifetimes at voltages V_1, V_2 and temperatures T_1, T_2, and E_a is an activation energy. This equation has shown itself useful for numerous MLC capacitor compositions, at least at lower voltages where values of n tend to range from 2.5 to 4 [37]. However, this was an empirical equation. Over the course of our project we have developed two theoretical derivations of equation 14, based on first principles. These are reviewed in Sec. 3.3.

We have found that the power law voltage dependence for degradation is followed for $BaTiO_3$-based Z5U and thick film capacitors, but not for X7R, which follow an exponential behavior. This is indicated in Figs. 20 and 21, for Z5U and X7R devices respectively.

The exponential temperature dependence of degradation rate β was satisfied by Z5U and X7R devices, with activation energies of 1.25 and 1.31eV respectively. This is shown in Figures 22 and 23.

3.2 Other Degradation Characteristics

In addition to the direct time dependent effects noted above, several other interesting changes in the properties of MLC devices occur as a result of accelerated degradation. These effects have also been discussed in the publications, which should be consulted for more details.

a) As device resistivity decreases during degradation, thermal activation energy decreases. This is seen in Figure 24 for an X7R device aged at 150°C, 400V. The exponentially increasing current is consistent with a linearly decreasing activation energy since $I \sim \exp(E_a/kT)$.

Figure 24 pertains to a single device. This trend applies to all 17 X7R devices that were degraded during a certain test early in the program: resistivity and activation decrease monotonically together. This is shown in Figure 25. This figure is consistent with Fig. 24 in that, for the upper points,

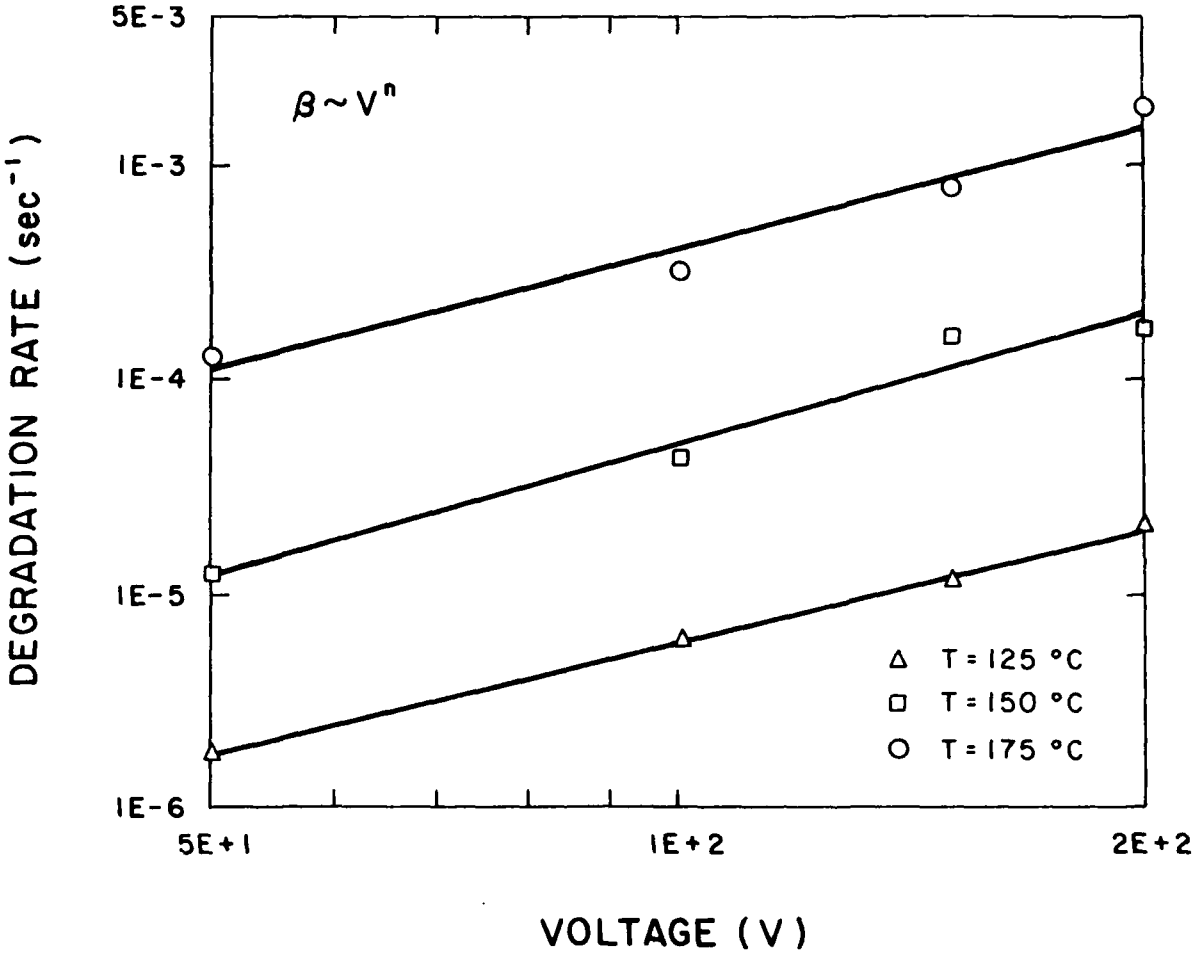

Figure 20. Power law voltage dependence of rate parameter β for Z5U degradation, at three temperature.

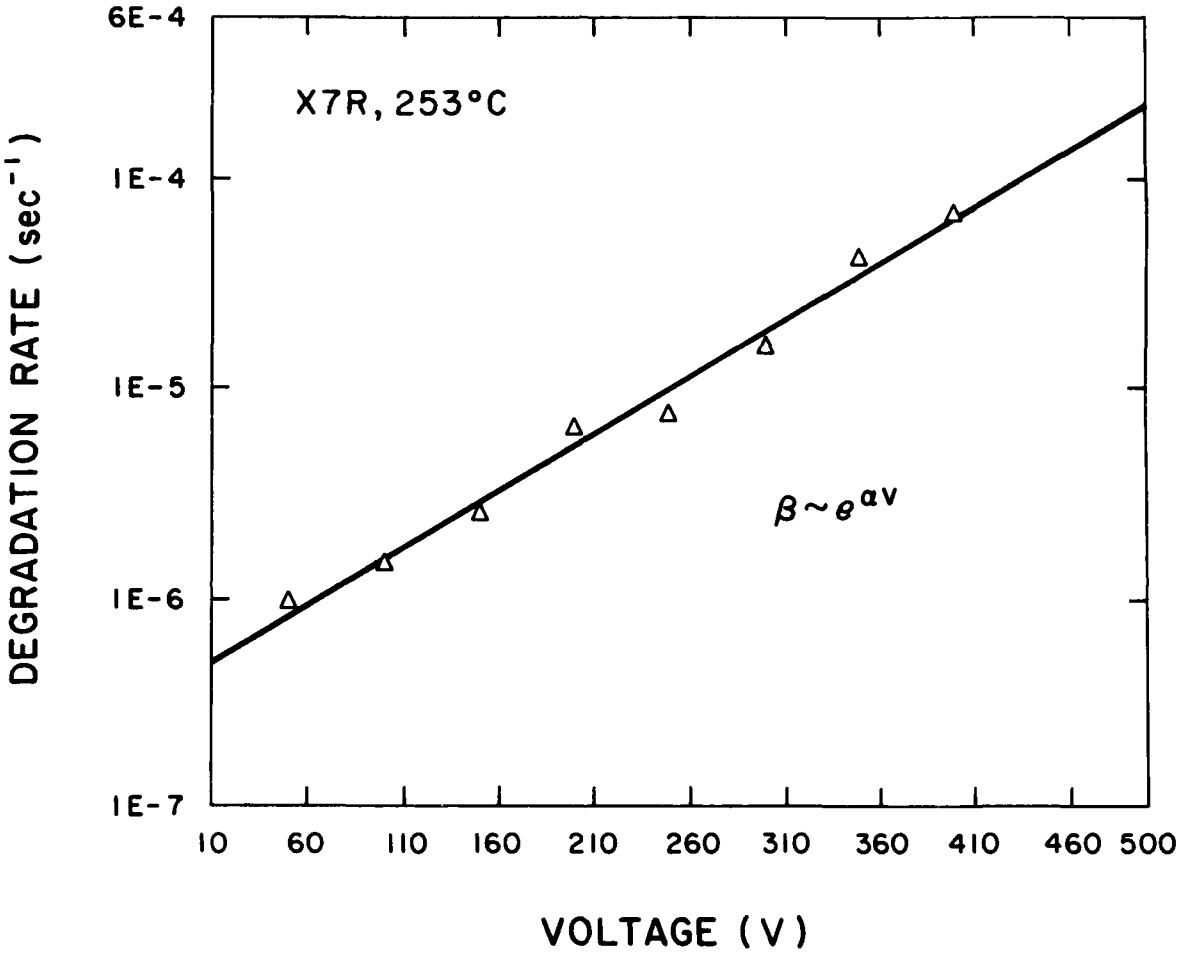

Figure 21. Exponential voltage dependence of rate parameter β for X7R devices.

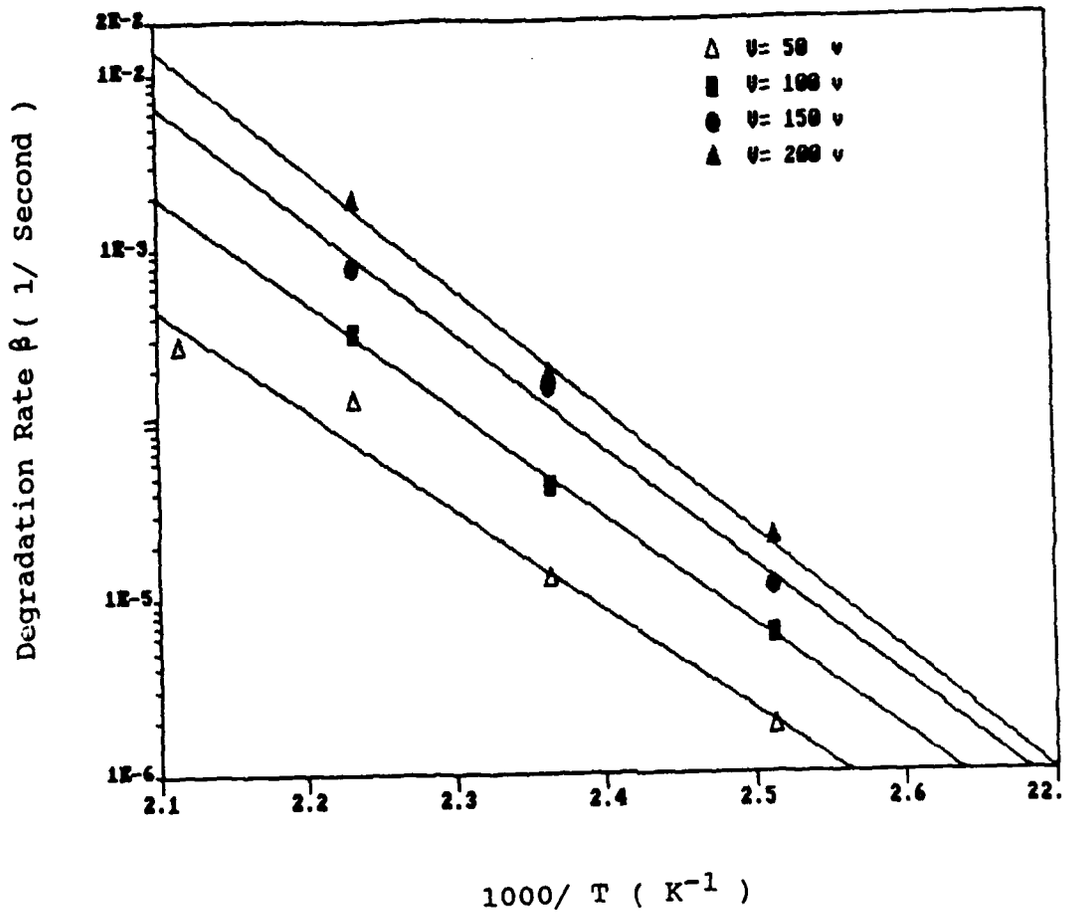

Figure 22. Arrhenius plot of temperature dependence of rate constant for Z5U devices at different voltages. Activation energy = 1.25 ± 0.1eV.

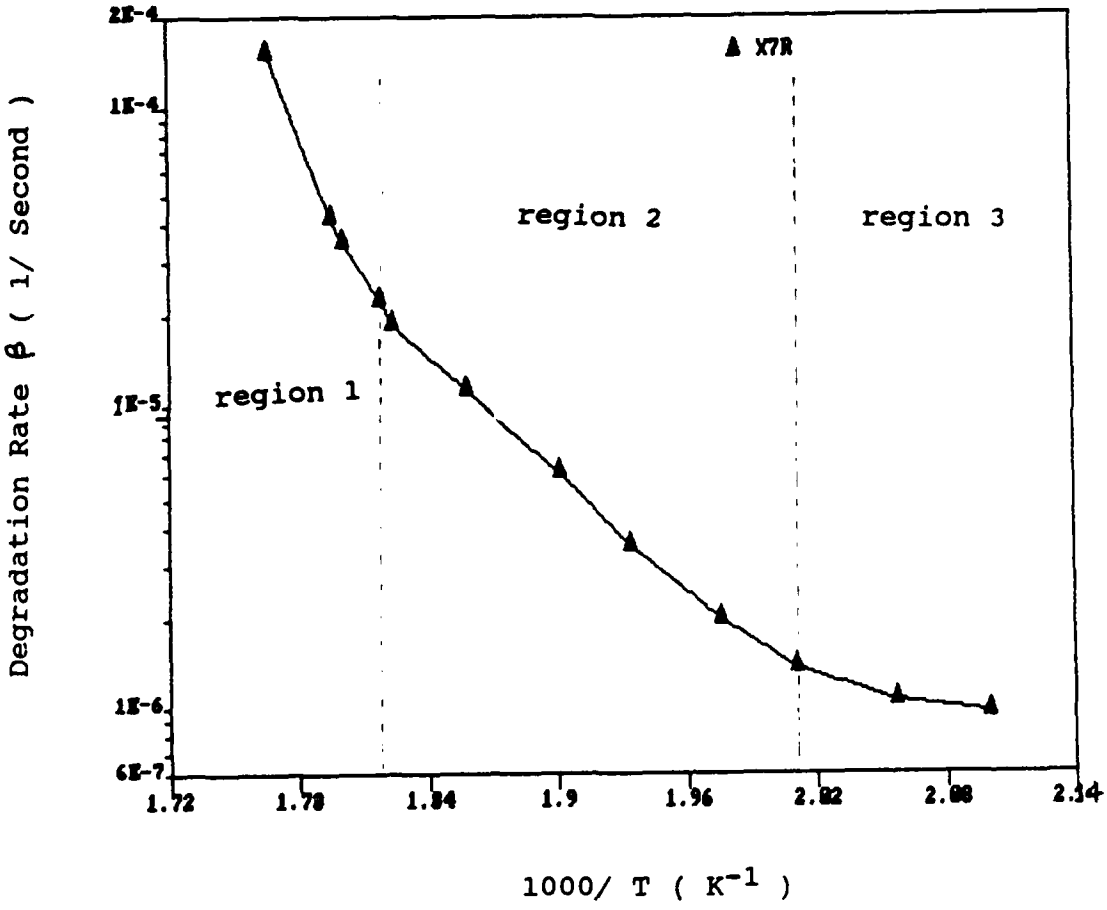

Figure 23. Arrhenius plot for temperature dependence of degradation rate for X7R at 200 volts. Activation energy in region 2 is 1.31eV.

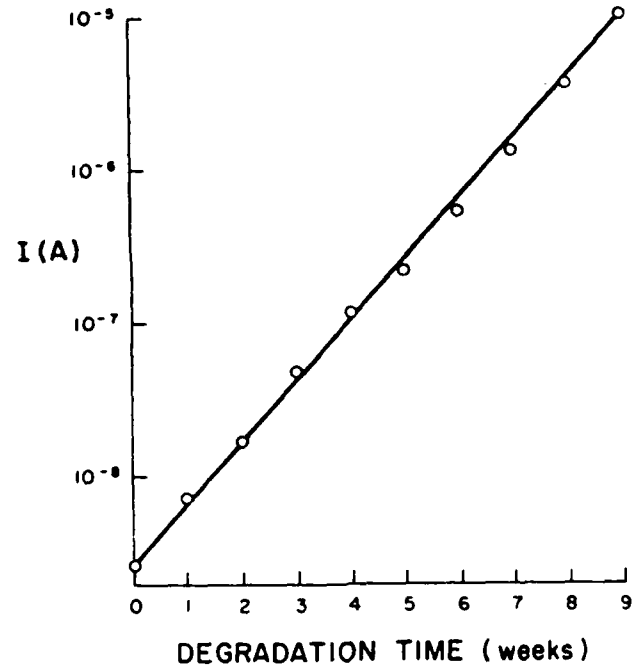

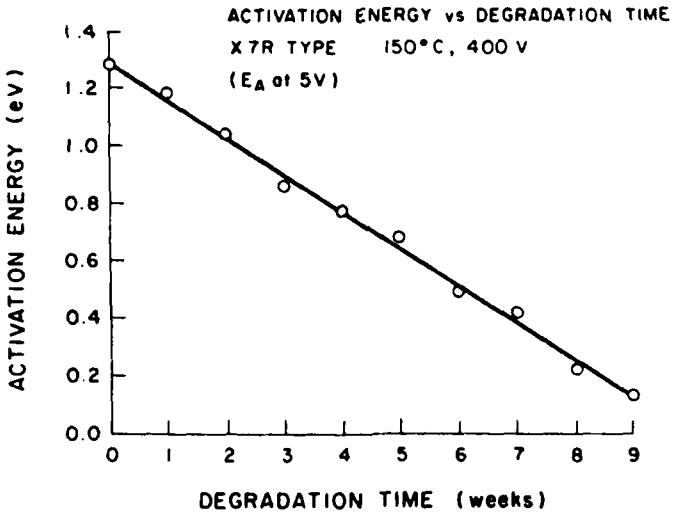

Figure 24. Exponential increase in current with time for an X7R device is accompanied by a linearly decreasing activation energy.

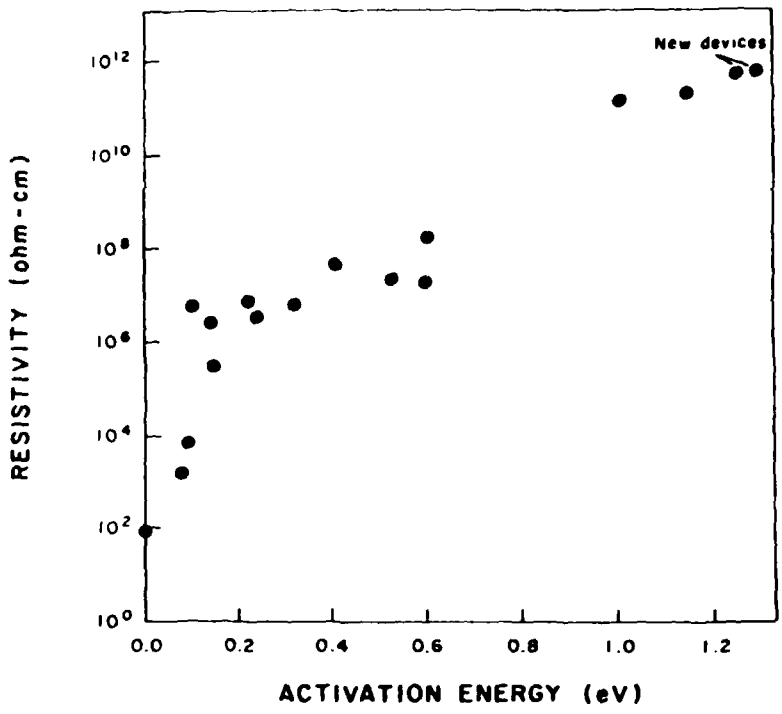

Figure 25. Dependence of resistivity (at 125°C) of degraded X7R devices on thermal activation energy.

resistivity increases roughly exponentially with activation energy. For the lower points (resistivity less than about $10^6\Omega$cm) activation energy approaches zero.

b) As ceramic resistivity decreases and leakage current increases, the I-V curve becomes more super-ohmic. For the device of Fig. 24, the voltage exponent increased from 1.25 to 1.65. If this test had proceeded longer, the exponent would have increased somewhat further, and then dropped to unity as the device approached failure. We have discussed this chronological evolution of I-V characteristics with degradation elsewhere [4]. One possible mechanism is a weakening of electron emission from electrode asperities with time, as the resistivity of the ceramic region near the asperity tip decreases, due to accelerated ionic migration in the enhanced field near the tip.

c) As discussed previously for "virgin" samples, the activation energy for reduced or degraded samples resides almost entirely in the mobility. (Figure 10, and Table 3). It is seen in these figures that, with reduction in hydrogen, carrier concentration and mobility can both be increased by orders of magnitude. According to the models discussed later, hydrogen reduction represents simulated degradation under voltage-temperature stress because both involve loss of oxygen.

d) We found and reported color gradients that developed across layers of stressed Z5U devices [1,4]. This could be due to ionic movement. Some interesting time-dependent polarity-reversal effects were also seen for Z5U capacitors (Fig. 26). Exponential or near-exponential current increases with time are evident. In Fig. 26a it is seen that a Z5U device whose leakage current increases by two orders of magnitude heals back to near its original state when the voltage is removed for 20 hours. As seen in Fig. 26b, a faster healing can be produced by reversing voltage polarity. Such healing effects are

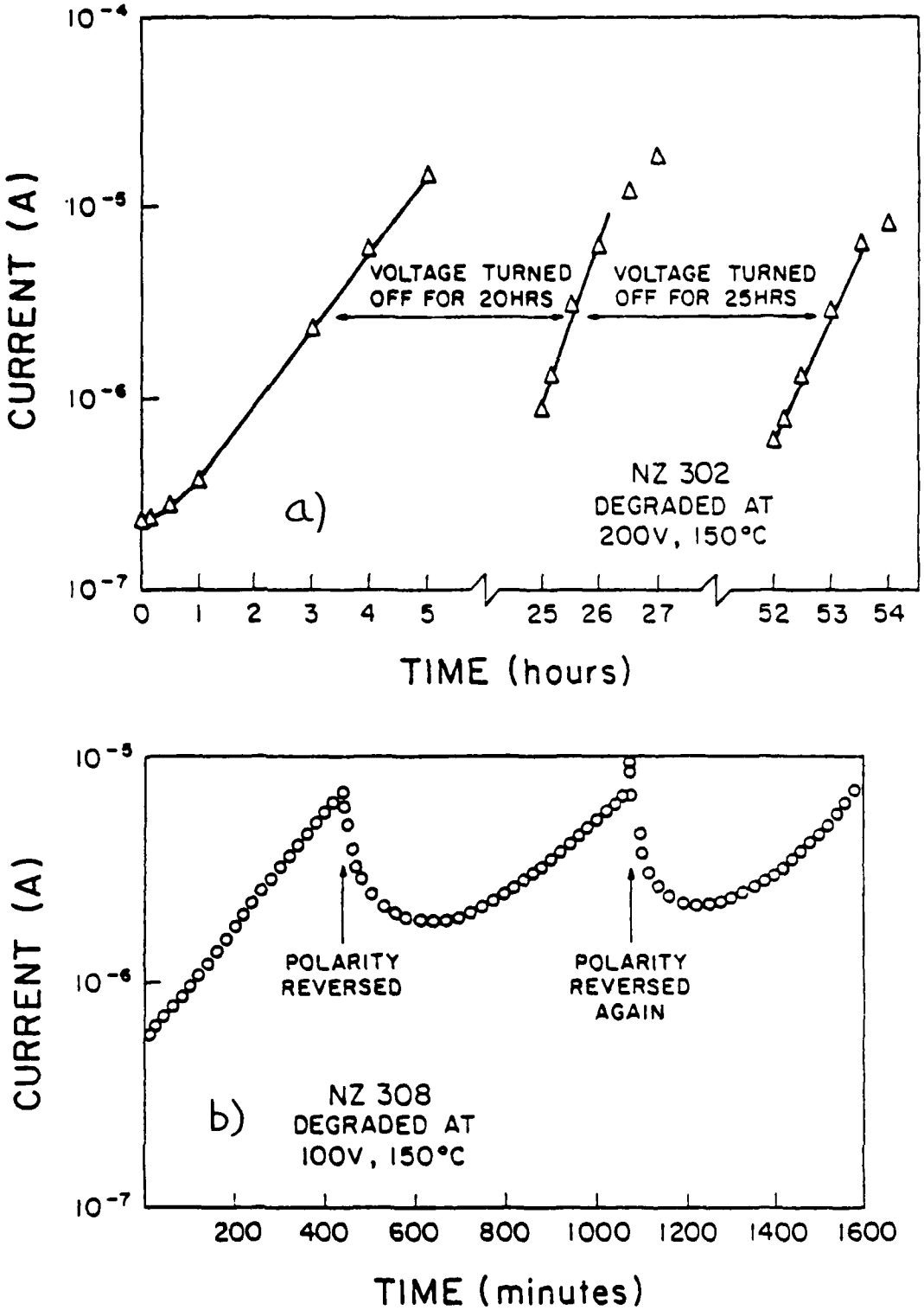

Figure 26. Time dependence of leakage currents for Z5U devices, showing healing effects. a) Resulting from removal of bias. b) Resulting from polarity reversal.

indicative of ionic movement and accumulation, and of a large conductivity gradient across the layer, both of which can be repaired to a large degree by polarity-reversal (with similar degradation subsequently occurring in the other direction.)

It is of interest that many of these degradation effects may be so fundamental as to apply to a variety of dielectric materials (exponentially increasing current, near-linearly decreasing activation energy, polarity-reversal healing, etc.) As an example, such behavior is illustrated in Fig. 27 for $BaTiO_3$-based, K=500 thick film capacitors, in the context of another program [34]. Such phenomena can be accounted for by ionic movement, as described in the next section.

3.3 Models for Degradation

We have developed and reported two models to account for the degradation phenomena that have been seen. The first one is based on oxygen ion and vacancy migration, leading to an increase in conduction electron concentration, and degradation [3,6]. The second is based on a time-dependent reduction of grain boundary barrier height, resulting in increased mobility, and degradation [34]. Since the role of grain boundaries in high-K ceramic has not been conclusively established, and since the grain boundary degradation model also depends on ionic movement, only the ionic movement model is reviewed here. We feel that such a model might pertain directly to accelerated voltage-temperatures degradation phenomena seen in high-K ceramic, and probably to many other dielectric types as well.

In this model, there are assumed to be two sources of conduction electrons: a "background" concentration resulting from impurities and defects in the as-made material, and electrons resulting from the generation of oxygen

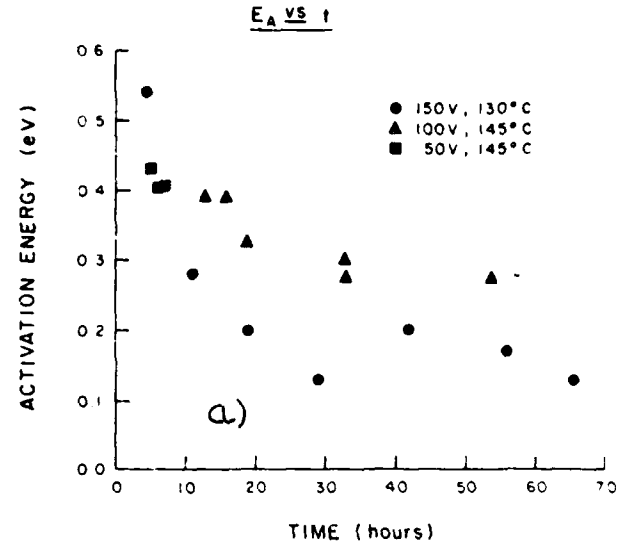

Activation energies versus degradation time for three samples aged under indicated conditions.

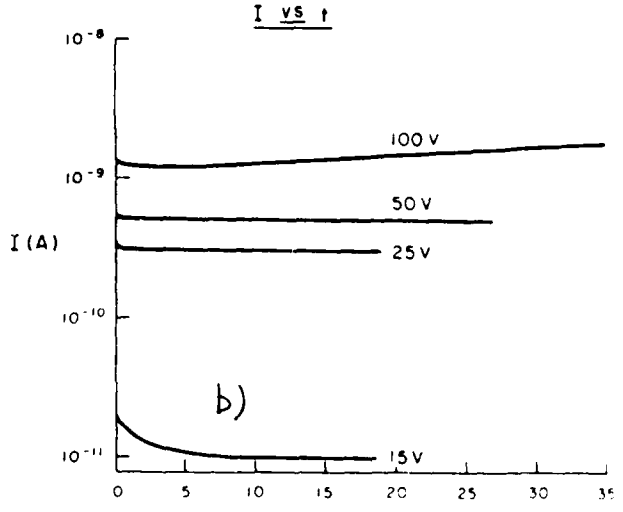

Leakage current versus time at four voltages (T = 120°C)

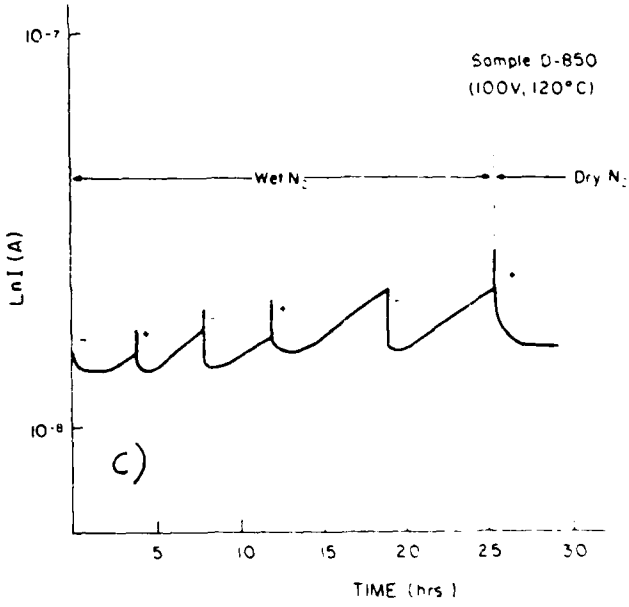

Healing effect by reversing polarity

Figure 27. For K = 500 thick film capacitors: a) Decrease in activation energy with degradation; b) Increase in leakage current; c) Healing by means of polarity reversal.

vacancies during degradation. The generation of electrons and vacancies is described by equation (5), with the electron density thus becoming equal to $2[V_{\dot{O}}\cdot]$ (plus the background concentration, which is ultimately neglected.) The oxygen vacancy current can be expressed in two forms, for a sample of cross section A and thickness W [6]. These are:

$$I_{ion} = 2qWA \frac{d}{dt}[V_O^{\cdot\cdot}] \tag{15}$$

and

$$I_{ion} = 2qA\mu_i \frac{V}{W}[V_O^{\cdot\cdot}] \tag{16}$$

Equation (15) says that the ionic ($0^{=}$) current is proportional to the time rate of increase in oxygen vacancy concentration. This assumes that none of the ions that leave are replenished from elsewhere.

Equation (16) assumes that oxygen ion transport in the solid is ohmic, where V is voltage and μ_i ion mobility. This assumption gives a voltage power-law dependence for degradation that is too low, which can be increased by assuming super-ionic transport for the ions, which results in a voltage exponent greater than unity.

Equating equations (15) and (16) we get

$$\frac{d[V_O^{\cdot\cdot}]}{dt} = \frac{\mu_i V}{W^2}[V_O^{\cdot\cdot}] \tag{17}$$

It is now assumed in the degradation regime that conduction election concentration $n_e = 2[V_{\dot{O}}\cdot]$. Equation (17) is then integrated to yield

$$n_e(t) = n_o e^{\beta t}, \qquad \beta = \frac{\mu_i V^n}{W^2} \tag{18}$$

where n_o is the background electron concentration and n is the super-ohmic voltage parameter mentioned earlier.

The empirical result reported earlier by others [35,36] can be obtained by defining lifetime τ as equal to β^{-1}, and assuming that ionic mobility μ_i is thermally activated, i.e. $\mu_i = \mu_o \exp[-E_a/kT]$. Lifetime τ can then be written

$$\tau = \beta^{-1} = W^2 \frac{e^{E_a/kT}}{\mu_o V^n} \tag{19}$$

The ratio of lifetimes for devices aged under different voltage and temperature conditions is

$$\frac{\tau_1}{\tau_1} = \left(\frac{V_2}{V_1}\right)^n \exp\left[\frac{E_a}{k}\left(\frac{1}{T_1} - \frac{1}{T_2}\right)\right] \tag{20}$$

Equation (20) agrees with our results for Z5U devices and with the empirical lifetime equations reported by Procopowicz and Vaskas [35], and by Minford [36].

References

1. L. C. Burton, "Intrinsic Mechanisms of Multi-Layer Ceramic Capacitor Failure", Annual Report, ONR Contract No. N00014-83-K-0168, Virginia Polytechnic Institute & State University, April 1984.

2. L. C. Burton, "Intrinsic Mechanisms of Multi-Layer Ceramic Capacitor Failure", Annual Report, ONR Contract No. N00014-83-K-0168, Virginia Polytechnic Institute & State University, April 1985.

3. L. C. Burton, "Intrinsic Mechanisms of Multi-Layer Ceramic Capacitor Failure", Annual Report, ONR Contract No. N00014-83-K-0168, Virginia Polytechnic Institute & State University, April 1986.

4. H. Y. Lee, K. C. Lee, N. N. Schunke and L. C. Burton, "Leakage Currents in Multilayer Ceramic Capacitors," IEEE-CHMT Transactions, CHMT-7, 443, 1984.

5. L. C. Burton, "Voltage Dependence of Activation Energy for Multilayer Ceramic Capacitors," IEEE CHMT Transactions CHMT-8, 517 (1985).

6. Y. Lee and L. C. Burton, "Charge Carriers and Time Dependent Currents in $BaTiO_3$-Based Ceramic," IEEE CHMT Transactions, CHMT-9, 469 (1986).

7. H. Y. Lee and L. C. Burton, "Influence of Electrode-Ceramic Interface on MLC Leakage Current," Advances in Ceramics 19, 219 (1986).

8. H. Y. Lee and L. C. Burton, "Models for Electronic Conduction Across Ceramic Grain Boundaries," Materials Research Soc. Symp. Proc. 60, 179-189 (1986).

9. S. S. Villamil, H. Y. Lee and L. C. Burton, "The Resistance of Grain Boundaries in $BaTiO_3$-Based Ceramic," IEEE CHMT Transactions CHMT-12, 482 (1987).

10. T. C. Lewis, "High Field Electron Emission From Irregular Cathode Surfaces," J. Appl. Phys. 26, 1405 (1955).

11. R. M. Anderson and D. R. Kerr, "Evidence for Surface Asperity Mechanism of Conductivity in Oxide Grown on Polycrystalline Silicon," J. Appl. Phys. 48, 4834 (1977).

12. H. R. Huff, R. D. Halvorson, T. L. Chin and D. Guterman, "Experimental Observations on Conduction Through Polysilicon Oxide," J. Electronchem. Soc. 127, 2482 (1980).

13. T. Hibma and H. R. Zeller, "Direct Measurement of Space Charge Injection from a Needle Electrode into Dielectrics", J. Appl. Phys. 59, 1614 (1986).

14. R. T. Thomas, "Time Dependence of the Electrical Conductivity of $BaTiO_3$ Single Crystals Heated in Oxygen," J. Phys. D: Appl. Phys. 3, 1434 (1970).

15. K. D. Schotte, "The Thermoelectric Properties of the Small Polaron," Zeit. fur Physik 196, 393 (1966).

16. P. Nagels, "Experimental Hall Effect Data for a Small-Polaron Semiconductor," in The Hall Effect and Its Applications, C. L. Chien and C. R. Westgate, eds. Plenum Press (1980).

17. W. Heywang, "Resistivity Anomaly in Doped Barium Titanate, J. Amer. Ceram. Soc. 47, 484 (1964).

18. L. M. Levinson, ed., Grain Boundary Phenomena in Electronic Ceramics, Amer. Ceram. Soc. (1981).

19. G. E. Pike and C. H. Seager, "The DC Voltage Dependence of Semiconductor Grain Boundary Resistance," J. Appl. Phys. 50, 3414 (1979).

20. G. D. Mahan and L. M. Levinson, "Theory of Conduction in ZnO Varistors," J. Appl. Phys. 50, 2799 (1979).

21. R. A. Smith, Semiconductors, sec. 6.2, Cambridge University Press (1964).

22. C. Pascual, J. R. Jurado, and P. Duran, "Electrical Behavior of Doped-yttria Stabilized Zirconia Ceramic Materials," J. Mater. Sci. 18, 1315 (1983).

23. L. Benguigi, "Space Charge Limited Currents in $BaTiO_3$ Single Crystals," Solid State Commun. 7, 1245 (1969).

24. L. Benguigi, "Electrical Phenomena in Barium Titanate Ceramics," J. Phys. Chem. Soc. 34, 573 (1973).

25. Y. V. Zabara, A. Y. Kudzin and K. A. Kolesnichenko, "Space Charge Limited Currents in Barium Titanate Single Crystals," Phys. Stat. Sol. (a) 38, K131 (1976).

26. A. Branwood, O. H. Hughes, J. D. Hurd and R. H. Tredgold,"Evidence for Space Charge Conduction in Barium Titanate Single Crystals," Proc. Phys. Soc. 79, 1161 (1962).

27. M. A. Lampert and P. Mark, Current Injection in Solids, Academic (1970).

28. A. Seuter, "Defect Chemistry and Electrical Transport Properties of Barium Titanate, Philips Res. Report Suppl. 3 (1974).

29. L. L. Kazmerski, Ed. Polycrystalline and Amorphous Thin Films and Devices, Academic (1980).

30. H. D. Park and D. A. Payne, "Characterization of Internal Boundary Layer Capacitors," in Grain Boundary Phenomena in Electronic Ceramics, Amer. Ceram. Soc. p. 242 (1981).

31. J. E. Bauerle, "Study of Solid Electrolyte Polarization by a Complex Admittance Method," J. Phys. Chem. Sol. 30, 2657 (1969).

32. M. Kleitz and J. H. Kennedy, "Resolution of Multicomponent Impedance Diagrams," in Fast Ion Transport in Solids, Vashishta, Mundy and Shenoy, eds., Elsevier (1979).

33. E. Schöll, "Lowering of Grain Boundary Barrier Heights by Grain Curvature, J. Appl. Phys. 60, 1434 (1986).

34. I. K. Yoo, L. C. Burton and F. W. Stephenson, "Electrical Conductor Mechanisms of Barium Titanate Based Thick Film Capacitors, IEEE Trans. Comp. Hybr. & Manuf. Technol., CHMT-10, 274 (1987).

35. T. I. Prokpowicz and A. R. Vaskas, "Research and Development, Intrinsic Reliability, Subminiature Ceramic Capacitors, Final Report, ECOM-90705-F, NTIS AD-864068 (1969).

36. W. J. Minford, "Accelerated Life Testing and Reliability of High K Multilayer Ceramic Capacitors," IEEE Trans. Comp. Hybr. & Manuf. Technol. CHMT-5, 297 (1982).

37. T. Zhang, "Electrical Conduction Transport Mechanisms of Barium Titanate Based Multilayer Ceramic Capacitors, MS Thesis, Materials Engineering Dept., VPI & SU (1988).

38. H. Bottger and V. V. Bryksin, Hopping Conduction in Solids, VCH Publishers (1985).

39. H. Y. Lee, "Electrical Transport Properties of Barium Titanate-Based Ceramics", Ph.D. Thesis, Materials Engineering Science, VPI & SU (1987).

40. M. P. Harmer et al., "The Effects of Composition and Microstructure on Electrical Degradation in $BaTiO_3$," Ferroelectrics 49, 71 (1983).

4. PROGRAM PARTICIPANTS

a. L. C. Burton - Principal Investigator, Professor of Electrical Engineering and Materials Engineering.

b. Kyo-Chol Lee - Visiting Research Scientist (1983-1984) from Ulsan Institute of Technology, South Korea.

c. Hee-Young Lee - Ph.D. Candidate (Degree received June 1987).

d. Neil Schunke - M.S. Candidate (Degree received June 1985).

e. Susan Villamil - M.S. Candidate (Degree received June 1987).

f. Tong Zhang - M.S. Candidate (Degree received August 1988).

g. Undergraduate Participants Debra Dorer

Scott Ottinger

Janet Henry

Kenneth Boggs

Imran Sherif

Sanjay Agarwal

h. Eric Ellis - Laboratory Technician

i. Kathy Taszarek - Secretary

5. PAPERS AND PUBLICATIONS

1. "The Resistance of Grain Boundaries in $BaTiO_3$-Based Ceramic," S. S. Villamil, H. Y. Lee, L. C. Burton, IEEE CHMT Transactions CHMT-12, 482 (1987).

2. "Models for Electronic Conduction Across Ceramic Grain Boundaries," H. Y. Lee and L. C. Burton, Materials Research Soc. Symp. Proc. 60, 179-189 (1986).

3. "Charge Carriers and Time Dependent Currents in $BaTiO_3$-Based Ceramic," H. Y. Lee and L. C. Burton, IEEE CHMT Transactions, CHMT-9, 469 (1986).

4. "Influence of Electrode-Ceramic Interface on MLC Leakage Current", H. Y. Lee and L. C. Burton, Advances in Ceramics 19, 219 (1986).

5. "Electrical Characterization of Ceramics and Polymers," L. C. Burton, Advances in Materials Characterization (ed. by R. Snyder, R. Condrate and P. Johnson), pp. 349-357, Plenum Press (1985).

6. "Voltage Dependence of Activation Energy for Multilayer Ceramic Capacitors," L. C. Burton, IEEE CHMT Transactions CHMT-8, 517 (1985).

7. "Leakage Currents in Multilayer Ceramic Capacitors," IEEE-CHMT Transactions, CHMT-7, 443, 1984 (with H. Y. Lee, K. C. Lee, J. N. Schunke).

8. "The Physics of Leakage Currents in Thin Insulating Ceramic Layers," L. C. Burton, Society for Advancement of Material and Process Engineering, Santa Clara, CA, June 1987 (Proceedings p. 495-502.

9. "Role of Grain Boundaries in MLC Capacitors," (L. C. Burton S. S. Villamil and H. Y. Lee), 37th Electronic Components Conference, Boston, May 1987 (Proceedings pp. 118-121).

10. "Models for Electronic Conduction Across Ceramic Grain Boundaries," Materials Research Society Symp. Proc. Vol. 60, p. 179-189 (1986).

11. "Grain Boundary Impedance in Ferroelectric Ceramic," 1986 IEEE International Symposium on Applications of Ferroelectrics, Lehigh Univ., June 1986, with H. Y. Lee and S. Villamil.

12. "Physics of Leakage Current in Thin Insulating Ceramic Layers," Engineering Foundation Conference "Ceramics in Electronics," Santa Barbara, CA (March 1986).

13. "Modelling of Leakage Current for High Resistance Ceramic," 1986 Annual Meeting American Ceramic Society, Chicago, (April 1986) with H. Y. Lee.

14. "Charge Carriers in MLC Capacitor Ceramic," 36th Electronic Components Conference, Seattle (May 1986) -- with H. Y. Lee.

15. "Voltage Dependence of Activation Energy for Multi-Layer Ceramic Capacitors," 35th Electronic Components Conference, Washington, D.C., May 1985.

16. "Grain Boundary Controlled Current in Multi-Layer Ceramic Capacitors", presented at American Ceramic Society Annual Meeting (Cincinnati, May 1985).

17. "Influence of Electrode-Ceramic Interface on MLC Leakage Current", American Ceramic Society Electronics Division Meeting, Orlando, FL, Oct. 1985 (with H. Y. Lee).

18. "Models for Electronic Conduction Across Ceramic Grain Boundaries", 1985 Materials Research Society Symposium, Boston, Dec. 1985.

19. "Leakage Currents in Degraded Multilayer Ceramic Capacitors," 1984 34th Electronic Components Conference (New Orleans, May 1984).

20. "Models for Leakage Currents in Multilayer Ceramic Capacitors," American Ceramic Society Annual Meeting (Pittsburgh, April 1984).

21. "Electrical Characterization of Ceramics and Polymers," 2nd Conference on Advances in Materials Characterization, Alfred, NY (Aug. 1984).

22. "Electrical Transport Parameters of Ferroelectric X7R Ceramic," VACON '84, Blacksburg, VA, Oct. 1984 - with H. Y Lee.

23. "Metal-Dielectric Interactions in Thick Film Distributed Parameter Networks," American Ceramic Society Electronics Division, San Francisco, October 1984, (with A. A. Riad, F. W. Stephenson, K. Razzaghi).

24. "Electronic Transport in Ferroelectric Ceramic" ibid., (with H. Y. Lee, N. Schunke, K. C. Lee).